THE UNIVERSITY OF MICHIGAN

INDUSTRY PROGRAM OF THE COLLEGE OF ENGINEERING

ORDERING AND CREEP PROPERTIES OF Ni-Cr-Al-ALLOYS

Charles Milles Hammond

A dissertation submitted in partial fulfillment
of the requirements for the degree of
Doctor of Philosophy in the
University of Michigan
1959

May, 1959

IP-370

Doctoral Committee:

Professor Richard A. Flinn, Chairman
Professor Lawrence O. Brockway
Professor James W. Freeman
Professor Richard Schneidewind
Professor Clarence A. Siebert
Professor Lars Thomassen

ACKNOWLEDGEMENTS

I wish to express my appreciation to all those who have aided in this investigation and particularly to the following:

Professor Richard A. Flinn, Chairman of the Doctoral Committee, for his encouragement, invaluable suggestions, and critical analyses during the course of this investigation.

Professors James W. Freeman and Lars Thomassen, members of the Doctoral Committee, for their friendly advice and helpful comments.

Professors Lawrence Brockway, Richard Schneidewind, and Clarence Siebert, members of the Doctoral Committee, for their interest and cooperation.

Dr. Paul A. Flinn of the Westinghouse Electric Corporation for the basic design of the elevated temperature X-ray camera and his helpful suggestions during this research.

International Nickel Company, the Bureau of Aeronautics, and the Office of Naval Research for financial assistance during most of this work.

My fellow graduate students in Mettallurgical Engineering for their cooperation, assistance, and enlightening discussions.

The members of Professor James Freeman's High-Temperature Group for their assistance in the experimental program.

The Industry Program of the College of Engineering for the production of this thesis.

TABLE OF CONTENTS

TABLE OF CONTENTS (CONT'D)

LIST OF TABLES

LIST OF FIGURES

LIST OF FIGURES (CONT'D)

INTRODUCTION AND OBJECTIVES

The Ni-Cr-Al ternary system is the basis of most of the high strength and heat resistant nickel-base alloys, such as the Inconels and Nimonics. According to the literature[1], two mechanisms of strengthening are possible in these materials: 1) an order-disorder transformation in the nickel-chromium rich matrix, based upon Ni_3Cr, and 2) precipitation hardening with a second phase based upon Ni_3Al, γ'. It has been shown in other alloys that both of these mechanisms can exert potent effects upon resistance to deformation at elevated temperatures.[2-14,22]

The existence of the order-disorder transformation is, however, controversial. Indirect evidence of ordering has been obtained by specific heat and resistivity measurements of Ni-Cr and Ni-Cr-Al alloys[15-20] and by X-ray diffraction measurements of Ni-Cr-Al alloys.[1] Neutron diffraction data disclosed no order-disorder transformation in Ni-Cr alloys.[21]

It is generally accepted that precipitation of the γ' phase controls, to a large extent, the creep-resistant characteristics of Ni-Cr-Al-base alloys.[6-14] However, the strengthening role of the proposed ordered matrix, based upon the ternary system, was not considered.

The objective of this research was, therefore, to investigate the controversial order-disorder transformation as well as γ' precipitation in the Ni-Cr-Al system and to correlate creep properties with the structural transformations disclosed. The alloy compositions selected for this research extended from Ni_3Cr to Ni_3Al. The existence of ordering was to be studied by elevated temperature and ambient temperature

X-ray diffraction. Optical and electron microscopy were to be used to ascertain the phases present during X-ray diffraction and creep studies.

The phase nomenclature used in this thesis is patterned after the work of Taylor and Floyd.[1] The symbol γ represents the solid solution rich in Ni and Cr and postulated ordered, based upon Ni_3Cr. The symbol γ' refers to the face-centered-cubic ordered phase based upon Ni_3Al. The γ' phase is a distinct precipitating phase which can be delineated clearly by electron microscopy.

REVIEW OF THE LITERATURE

The literature pertinent to this investigation may be classified, for convenience, into the following two categories: the order-disorder transformations in the Ni-Cr-Al system and the influence of ordering and γ' precipitation upon elevated temperature properties.

The Order-Disorder Transformations

The order-disorder transformations proposed in Ni-Cr-Al alloys were initially postulated in the Ni-Cr and Ni-Al binary systems. Therefore, the literature review of the order-disorder transformations will be presented in the following sequence: the Ni-Cr, the Ni-Al, and the Ni-Cr-Al systems.

The Ni-Cr System

It has long been known that Ni-Cr alloys of composition Ni_3Cr exhibited anomalous resistance-temperature and specific heat-temperature relationships.[15-19] These anomalies have been tentatively ascribed to an order-disorder transformation although no direct X-ray diffraction evidence has been presented.[16,19]

The continuous resistance-temperature curves for this alloy do not follow the conventional relationship for an order-disorder transformation. The resistance increases during the proposed ordering rather than showing the conventional decrease as in Cu_3Au.[23-27] The specific heat-temperature curves are normal for an order-disorder transformation.

Taylor and Hinton[19] re-examined a Ni-Cr alloy (Ni_3Cr) and another alloy with 5 atomic percent Al replacing Cr and found an increase

in resistivity with ordering. Specific heat-temperature curves, however, were in agreement with a superstructure formation. Superlattice lines were not visible in the ordered Ni_3Cr material but were present in the Ni-Cr-Al alloy. Taylor and Hinton concluded that Ni_3Cr alloys possessed a highly ordered structure based primarily upon the specific heat data.

Masumoto and coworkers[28] measured specific heats of several Ni-Cr alloys and concluded that a Ni_3Cr compound existed. Kornilov and Mints[29] determined the change in electrical resistance, linear expansion coefficient, and lattice dimensions of several Ni-Cr alloys. A sharp minimum in the electrical resistance-atomic percent Cr curve, corresponding to 24 atomic percent Cr, indicated the formation of a Ni_3Cr compound. A similar minimum was discovered at 24 atomic percent Cr in the linear expansion coefficient. X-ray analyses showed a decrease in lattice parameter after annealing. The published equilibrium diagrams[30-39], however, do not indicate the existence of a Ni_3Cr compound.

Nordheim and Grant[20] measured equilibrium resistivities of Ni-Cr alloys (near Ni_3Cr) at several temperatures rather than determining continuous resistivity changes during heating and cooling. The equilibrium resistivity curves did not show any discontinuities at temperatures from 200-1000°C (392-1832°F) for alloys close in composition to Ni_3Cr. Specimens quenched from 980°C (1769°F) and annealed at lower temperatures showed an increase in resistivity as a function of time. The increase was dependent upon composition and temperature, being strongest for Ni_3Cr alloys and at 540°C (1004°F). Since superlattice lines and discontinuities in resistivity were absent in Ni_3Cr alloys, Nordheim and Grant concluded

that short range order rather than long range order explained the anomalous specific heat temperature curves. Hardness and resistivity measurements of isothermally annealed alloys after quenching, containing 32 and 35 percent Cr, indicated long range order, similar to CuAu, although no superlattice lines were identified.

Recently, Roberts and Swalin[21] investigated the Ni-Cr system, in the vicinity of Ni_3Cr, with neutron diffraction and dilatometric measurements. Neutron diffraction is favorable for detection of a superlattice in this system because of the differences in coherent amplitudes of Ni and Cr in a neutron beam ($_{28}$Ni-10.2, $_{13}$Cr-3.52). The authors found neither distinct superlattice lines nor diffuse scattering and concluded that long range and short range order were absent in the Ni-Cr system near the atomic composition Ni_3Cr. No dimensional changes occurred in a quenched specimen aged for long periods of time at temperatures where ordering had been indicated by changes in resistivity and specific heat.

The Ni-Al System

Most of the investigators of the Ni-Al system[40-47] identified two ordered structures: Ni_3Al (γ') and NiAl (β). Ni_3Al has an ordered face-centered cubic structure similar to Cu_3Au. NiAl has an ordered body-centered cubic CsCl-type structure. Ni_3Al is considered to be ordered to the melting point, 1400°C (2552°F).

The Ni-Cr-Al System

The Ni-Cr-Al ternary system was investigated by Taylor and Floyd.[1] X-ray evidence, from samples of alloys quenched from within

the single phase γ field, showed that the order-disorder transformation, indicated by specific heat and resistivity anomalies in Ni-Cr alloys and dilute Ni-Cr-Al alloys, persisted to 1150°C (2102°F) when the aluminum content was greater than 10 atomic percent. Therefore, the ordering temperature of the γ solid solution apparently increases from 540°C (1004°F) at Ni_3Cr to approximately 1400°C (2552°F) at Ni_3Al.

The Relation of Ordering and γ' Precipitation to Elevated Temperature Properties

Effect of Ordering Upon Elevated Temperature Properties

Theoretical and experimental evidence indicate that ordering has a potent effect upon elevated temperature properties of other alloys. No experimental evidence is published concerning creep properties of ordered Ni-Cr-Al alloys.

Theoretical Evidence.--Fisher[2] and Cottrell[3] showed that short range and long range ordering should result in an increase in resistance to plastic deformation because of the interaction between dislocations and anti-phase domain boundaries. The shear stress necessary to overcome the repelling action of the domain boundary and the dislocation is:

$$\sigma = \gamma/b$$

where σ is the shear stress, γ the surface tension of the domain boundary, and b the burgers vector. This shear stress is in addition to the shear stress required to move a dislocation if the atom distribution is random.

Experimental Evidence.--Research in the Ni-Fe system by Kornilov[4] showed that the creep resistance markedly increased near the atomic composition Ni_3Fe at temperatures above and below the critical temperature for ordering. Herman and Brown[5] determined that the creep resistance of β brass increased due to ordering.

Effect of γ' Precipitation Upon Elevated Temperature Properties

The initial development of the Nimonic-type nickel-base alloys by Pfeil and coworkers[6] showed that additions of titanium and aluminum to 80 nickel-20 chromium alloys markedly enhanced hardness and creep-rupture properties. Hignett[7] mentioned that the hardening of Nimonic 80 was due to controlled precipitation of $Ni_3(Al,Ti)$, having a Ni_3Al structure. An extensive investigation of Nimonic alloys by Nordheim and Grant[8] confirmed the statement of Hignett. French investigators[9,10] concluded that a submicroscopic precipitate existed in heat-resistant nickel-chromium alloys and that the best elevated temperature properties were obtained with the smallest mean free path between particles.

Frey and coworkers[11] identified a precipitate in Inconel X and correlated creep properties with aging times. For the lower aging temperatures investigated, maximum properties occurred at particle spacings which agreed with the theoretical calculations of Mott and Nabarro.[12] Later Brockway and Bigelow[13] identified the precipitate in Inconel X as γ' (Ni_3Al) and confirmed the particle measurements of Frey.

Betteridge and Smith[14] suggested, from comparative tests on three heats of Nimonic 90, that the highest stress-rupture properties were obtained with the greatest content of precipitated phases. On the other

hand, work on Nimonic 80A by the same authors showed that no inflection of the rupture stress-temperature relation occurred when the structure changed from a matrix solid solution plus a dispersed γ' phase to a complete solid solution. It was suggested that the conflicting results obtained from Nimonic 90 and 80A could be reconciled by assuming that the increase in stress rupture strength due to the formation of a precipitated phase was, in the case of Nimonic 80A, sufficient only to compensate for the decrease in strength due to the loss of the precipitated material from the solid solution.

Recently, Weertman[22] suggested that particle size as well as interparticle spacing and volume percentage controlled creep resistance. The inclusion of particle size effects is based upon the theory of dislocation climb as the mode of creep deformation.

Summary of Literature Review

It is evident that considerable controversy exists concerning the order-disorder transformation, based upon Ni_3Cr, in the Ni-Cr-Al system. Indirect evidence of ordering by resistivity and specific heat measurements in Ni-Cr alloys is contradicted by neutron diffraction results. X-ray confirmation of ordering in Ni-Cr-Al alloys based upon quenched specimens, further clouds the issue.

The two strengthening mechanisms, ordering and precipitation hardening, can markedly affect creep resistance. No data are available distinguishing between the effects of these possible strengthening mechanisms in simple Ni-Cr-Al alloys.

Therefore, it was decided to investigate the controversial order-disorder transformation as well as the precipitation of γ' in the Ni-Cr-Al system in order to correlate creep properties with the structural transformations.

EXPERIMENTAL PROCEDURES

To develop the proper background for the structures controlling the elevated temperature properties of Ni-Cr-Al alloys, an investigation of the phase equilibria was performed. Following this, elevated temperature properties of representative alloys were evaluated.

The phase studies included a preliminary investigation of the Ni-Cr-Al ternary diagram at compositions extending from Ni_3Cr to Ni_3Al. The proposed order-disorder transformation was explored by elevated temperature and ambient temperature X-ray diffraction. Optical and electron microscopy were used to supplement the X-ray data.

The mechanical properties of representative alloys were determined primarily from wrought material. A single phase alloy and two alloys with different dispersions of γ' were used in this investigation of mechanical properties.

A detailed description of the various procedures follows. The descriptions are given in the sequence in which the data were obtained, namely, preparation of experimental materials, chemical analyses, heat treatments, X-ray diffraction techniques, mechanical properties, and metallography. This section will be concluded with a presentation of the phase diagram studies.

Preparation of Experimental Materials

The alloys were poured in investment molds in the first part of the investigation since plans called for cast test bars. (Because of shrinkage problems ingot molds were used later to produce material for wrought test bars.) Sections of the gating system of the investment

casting were processed by hot and cold rolling to produce specimens for phase studies.

Investment Molding

Cast test bars were made by the lost-wax investment casting process. A photograph of a pattern cluster of wax tensile bar patterns is shown in Figure 1. The actual gage length is 0.250 inches in diameter and one inch long. The pins projecting from the shoulders of the specimens were produced as an integral part of the castings to facilitate subsequenct attachment of the extensometers during elevated temperature testing. Each bar was individually risered.

The wax clusters were dipcoated and invested with a refractory slurry of the ethyl silicate-type. After hardening, the molds were dewaxed at 121°C (250°F). The firing temperature was 982°C (1800°F) preparatory to pouring.

Melting

All material prepared for this research was vacuum melted in the apparatus shown in Figure 2. The furnace capcity was approximately 10 pounds and alumina crucibles were used. Prior to melting, the alumina curcibles were outgassed in the vacuum chamber. The pressure during melting was maintained between 1-5 microns. The general melting procedure was the same for all heats but the pouring procedure was different for casting ingots and investment molds. The metal melted varied from six to nine pounds.

The heats melted, intended analyses, raw materials, and special additions are shown in Table I. The boron was added to R 447 and 448 to facilitate hot rolling. (Heats made without boron cracked badly during

rolling. This "scavenging" addition has long been standard furnace practice for nickel alloys.) The chromium was always completely charged into the crucible. The remainder of the charge was nickel. The crucible charge was usually melted twenty minutes after power application. The remainder of the nickel was added slowly to avoid splashing. Fifteen minutes were allowed for refining after melt-down. The aluminum and nickel-boron were added slowly with the power on so that maximum mixing occurred. When ingots were cast, the metal temperature, as measured through a long sight tube with an optical pyrometer, was increased to 149°C (300°F) above the freeze point and poured. The cast ingot size was 2-3/8 inches in diameter by 7 inches high.

A more elaborate pouring procedure was necessary to cast hot investment molds. After all additions were made, the melt was frozen, argon was bled into the vacuum chamber to open it, a cover was placed over the crucible, and the hot investment mold inserted. The chamber was evacuated to 2 millimeters before the power was again applied. The pressure was approximately 50 microns before the heat was molten. The heat was poured when the metal was superheated 149°C (300°F). The entire operation usually required 8-10 minutes. During this time, the temperature of the investment mold decreased to approximately 871°C (1600°F) according to thermocouple measurements in the mold cavity. The molds were kept in the vacuum chamber until the castings solidified.

Wrought Specimens for Phase Studies

Sections of the ring gate of the investment castings were hot-rolled to produce fine grained specimens for phase studies. The grain size of the as-cast material was too coarse for good X-ray diffraction

patterns. The material was homogenized at 1204°C (2200°F) for two hours prior to hot rolling. The reductions per pass were approximately 10 percent, with 10 minute reheats after each pass. The initial and final thicknesses were 1/2 and 1/8 inches respectively. These specimens were used for determination of the solvus line, for ordering determinations by X-ray diffraction of quenched specimens, and as stock for foil specimens used in elevated temperature X-ray diffraction.

The foil specimens were prepared by the research laboratory of the Westinghouse Electric Corporation. The 1/8 inch thick hot-rolled specimens were cold rolled, with intermediate anneals, to a thickness of approximately 0.001 inch. Processing of most of these materials was extremely difficult because of susceptibility to cracking.

Wrought Specimens for Determination of Mechanical Properties

Ingots were homogenized 12 hours at 1204°C (2200°F) prior to hot rolling. The reductions per pass were 3-5 percent, with 10 minute reheats per pass for a total of 25 passes. The final bar size was 1-1/4 inches square by 9 inches. The rolled bars were quartered and cut into three-inch lengths generating eight test bars per ingot. The quartered bars were heat-treated and machined into test bars according to ASTM specifications.

Chemical Analyses

All heats were analysed for nickel, chromium, and aluminum. Important heats for property investigations were analysed for other elements such as carbon, nitrogen, and boron. These analyses are included in Table II.

Aluminum and chromium analyses were performed on randomly selected pieces of foil from the same heat to determine whether the composition was uniform from sample to sample. The analyses were conducted on a comparative basis by X-ray flourescence. The samples were judged uniform with respect to nickel, chromium and aluminum.

Heat Treatments

Thermal treatments were necessary for several phases of this research. The furnaces used included globar-types and conventional resistance furnaces. All furnaces were checked for temperature gradients. Temperatures were checked with thermocouples placed next to the specimens. The maximum temperature fluctuation was $\pm$ 4°C ($\pm$ 10°F). The specimen size for phase studies was 1/2 x 1/2 x 1/8 inches. No protective atmospheres were used unless noted later in the text.

The special heat treating techniques employed will be presented under the following headings: Phase Diagram Studies, X-ray Diffraction Studies and Investigation of Mechanical Properties.

Phase Diagram Studies

Cast and wrought specimens were used to investigate the phase diagram. The cast specimens were initially homogenized at 1204°C (2200°F) for four hours and air cooled.

The homogenized cast material and wrought specimens of heats R 332, 333, 334, 379, 380, 346, and 347 were heat-treated at various temperatures for 12 to 24 hours. The 12 hour treatments were used above 1000°C (1832°F), 24 hour treatments below 1000°C (1832°F). These times were dictated by times necessary for stable temperature measurements from elevated temperature X-ray diffraction specimens.

The specimens were supported from the furnace hearths by alundum boats. The specimens were quenched with the boats into an ice-brine bath at the end of the heat treatment. The transfer time was approximately one second.

X-Ray Diffraction Studies

Solid specimens of R 332, 333, 334, 379, 380, 346, and 347, for X-ray diffraction measurements, were quenched into ice-brine from both the single and two phase fields of the equilibrium diagram. All specimens used to determine the phase diagram were quenched from furnaces with horizontal hearths. The transfer time was approximately one second.

Samples of heat R 380 were quenched into various media from a vertical tube furnace to investigate γ' precipitation during quenching. The quenching baths were ice-brine, water, oil, and air. The specimens dropped approximately 18 inches before reaching the quenching bath. The approximate transfer time was one-tenth second.

Heat treatments for precision lattice parameter measurements involved a differenct procedure. Filings of solution-treated and aged specimens from R 437, 436, and 438 were prepared and placed into fused silica tubing. The fused silica tubing was evacuated and the ends sealed. The capsules were aged at 750°C (1382°F) for one hour. The unbroken capsules were quenched into an ice-brine bath. No reaction between the filings and fused silica was observed.

Investigation of Mechanical Properties

A few differences existed in the heat treatments of the cast and wrought specimens.

All of the thermal treatments of cast test bars were performed in a protective atmosphere of argon. The cast bars were initially homogenized and solution-treated at 1178°C (2150°F) for 12 hours and air-cooled. The solution-treated bars from heats R 436 and 437 were aged at 750°C (1382°F) for 100 and 24 hours respectively. The solution-treated bars from heat R 438 were given a double aging treatment of 954°C (1750°F) for 24 hours, furnace-cooled to 750°C (1382°F), and aged at 750°C (1382°F) for 24 hours and air-cooled.

The wrought bar stock of heats R 447 and 448 was solution-treated at 1000°C (1832°F) for 12 hours and air-cooled. All bars of R 447 were aged at 750°C (1382°F) for 24 hours and air-cooled. Bars 1, 2, 3, and 8 of R 448 were aged at 871°C (1600°F) for 24 hours and furnace-cooled to 750°C (1382°F) and aged at 750°C (1832°F) for 24 hours and air-cooled. The remaining specimens of R 448 were aged at 750°C (1382°F) for 100 hours and air-cooled. All heat treatments are summarized in Tables III and IV.

X-Ray Diffraction Techniques

Elevated Temperature X-Ray Diffraction

Before presenting the procedures used in elevated temperature diffraction, the equipment will be described and the preliminary experiments discussed.

Description of Equipment.--The diffraction apparatus consists of the following components: X-ray, vacuum, and gas purification equipment. Figure 3 is a photograph of the apparatus and Figure 4 is a schematic diagram of the equipment, including X-ray geometry.

X-Ray Equipment.-The X-ray equipment is composed of a Machlett line-focus, chromium, diffraction tube, a monochromator, and a camera. The X-rays emerge from the tube ports at a 6° angle. The beam is collimated by molybdenum slits before entering the monochromator.

The monochromator is made of a curved single crystal of fluorite with the (111) plane parallel to the crystal surface. A fluorite crystal was selected to minimize the second and third order reflections. The crystal was cleaved to 0.150 inches, polished to 0.012 inches, and glued with epoxy resin to a brass block with a radius curvature of 17.9 inches. The geometry of the monochromator requires that the crystal be bent to a radius twice that of the focusing circle. For perfect focus, an arc of radius equal to the radius of the focusing circle must be cut from the bent crystal. The latter operation was not performed because of the difficulties in machining thin fluorite resulting in some loss of efficiency of the monochromator.

The X-ray camera is shown in Figure 5. The front of the camera houses the heating chamber and the back section the diffraction area. Beryllium windows, sealed to the camera with resins and glyptal, serve as entrance and exit ports. The film is on the outside of the camera in a light-tight paper holder. The specimen, a foil roughly 1-1/2 x 1/4 x 0.001 inches, is heated by an AC electric current. A small piece of titanium foil, suspended from the camera top and not reached by the X-ray beam, serves as a getter during the exposure. The camera is sealed, evacuated to 0.01 micron of mercury, and finally refilled with 600 millimeters of purified helium prior to heating the specimen.

Vacuum Equipment.-The camera is evacuated by an oil-sealed mechanical pump and mercury diffusion pump. A liquid nitrogen cold trap was inserted between the camera and the vacuum pumps. The connections between the camera and the pumping system are glass. A thermocouple gauge, mounted in the camera, measures pressure and leak rate. The vacuum attainable in the system is below the sensitivity of the thermocouple gauge and is about 0.01 micron.

Gas Purification Equipment.-During the course of this investigation it was determined that at higher temperatures the composition of the foil changed by vaporization during the elevated temperature exposure. A purified helium atmosphere was used to suppress the vaporization. The helium was purified by passing the gas through activated charcoal at liquid nitrogen temperatures. The charcoal was re-activated by heating under vacuum.

Preliminary Experiments.--Preliminary experiments with elevated temperature X-ray diffraction of Ni-Cr-Al alloys indicated that temperature measurements and vaporization were problems to be overcome before reliable diffraction data could be obtained.

Temperature Calibration.-Initially platinum-platinum-10 percent rhodium thermocouples were spot-welded to the foil surface to measure temperatures. The thermocouple was finally eliminated because of alloying between the thermocouple wires and foil at higher temperatures and at times greater than 24 hours and because of thermocouple failures. Optical pyrometer measurements, made through a long sight tube, were then used to measure foil temperatures.

The optical pyrometer was calibrated by simultaneously measuring Ni-Cr-Al foil temperatures by thermocouple and optical pyrometer readings. (These experiments were of short duration and no alloying occurred between the thermocouple wires and foil.) The preoxidized foil was mounted in the holders in the camera top and heated in air. Simultaneous temperature measurements were recorded, Figure 6. A constant correction of 110°C is indicated for optical measurements. As a further check on these measurements, a piece of preoxidized iron foil (of black body characteristics) was heated in the camera and the α to γ transformation temperature was measured by X-rays and optical pyrometer readings. The transformation occurred at 1475°F (800°C) compared with the prediction of the equilibrium diagram, 1670°F (910°C). This corroborated the other measurements. Therefore, as a result of this investigation, a temperature correction of 110°C (200°F) was applied to all temperatures recorded by the optical pyrometer.

The foils, used as elevated temperature diffraction specimens, were preoxidized prior to inserting in the elevated temperature camera. The object of this treatment was to insure no change in foil emissivity during the long exposure (72 hours). The effect of the surface condition of the foil upon temperature measurements is shown in Figure 7. The temperature measurements from preoxidized foil and foil after exposure in the elevated temperature camera were similar and, therefore, no variations in emissivity occurred during heating at elevated temperatures. Theses measurements were made in a vacuum unit used for shadowing replicas for electron microscopy. This unit was used to minimize further oxidization of the foils during the measurements.

Vaporization.-Heating Ni-Cr-Al foils in a vacuum at 1073°C (1963°F) resulted in vaporization of aluminum and probably chromium from the foil surface. Figure 8 shows the vaporized surface of a foil of R 449 which was heated at 1073°C (1963°F) for 90 hours in a vacuum. The absence of γ' from the surface signified that vaporization occurred. The introduction of a pressure of approximately 600 millimeters of purified helium suppressed the vaporization as shown in Figure 9. (The rate of vaporization of a given alloy is directly proportional to total pressure.) This helium atmosphere of 600 millimeters was used in obtaining all elevated temperature diffraction data.

Helium was effective in suppressing vaporization at all temperatures for heats R 332, 333, and 334. Vaporization was troublesome in heat R 449 at temperatures greater than 1073°C (1963°F) with a helium atmosphere as shown by metallographic examination of exposed foil.

Three basic types of surface coatings were attempted to suppress vaporization above 1073°C (1963°F): anodizing the foil surface, coating the surface with a ceramic, and electroplating the surface with molybdenum and nickel. None of these techniques was successful.

Elevated Temperature X-Ray Diffraction Procedures.--The procedures involved were slightly different for the low aluminum (8.4-12.2 At.% Al) foils, R 332, 333, and 334 compared with the high aluminum foil, R 449 (16.1 At.% Al). The general procedures common to all foils will be presented first followed by specific techniques.

The cold-rolled foils were etched to remove surface oxides and to decrease the sample thickness to approximately 0.001 inch. The foils were weighed as-etched, after preoxidation, and after the exposure to

check for vaporization and oxidation. The preoxidized foils were inserted into the camera and a vacuum drawn. The titanium and sample foil were outgassed at approximately 815°C (1500°F). After a minimum pumping time of eight hours, the purified helium was bled into the camera to a pressure of 600 millimeters. The foils were heated to temperature, held for 12 or 24 hours, exposed, and quenched in the camera by quickly shutting off the power to the specimen. The foils were examined microscopically after the exposure. Debye powder patterns identified the surface oxides present. Integrated intensities for the (100) and (111) lines were measured on a Leeds and Northrup microphotometer.

The exposure temperatures referred to in the following sections are average values. The range was ± 18°C (± 30°F).

Low Aluminum Foils.-Prior to exposure at temperature, the foils of heats R 332, 333, and 334 (from 8.4 At.% - 12.2 At.% Al) were given a grain coarsening treatment at 1038°C (1902°F) for four hours. This treatment, along with lattice parameter determinations, distinguished the superlattice lines from the oxides of aluminum and chromium.

Foils of R 332 and 333 were investigated at 893°C (1640°F). This temperature is the lower limit of the optical pyrometer. This provided a satisfactory lower limit, however, because at this temperature both compositions were single phase.

Foils of R 334 were exposed at 893°C (1640°F), 982°C (1800°F) and 1038°C (1902°F). To determine whether vaporization occurred at the high temperature, 1038°C (1902°F), the following critical experiment was performed. Patterns were obtained at 1038°C (1902°F); then the foils

were aged at 893°C (1640°F) for 24 hours and the pattern obtained at 893°C (1640°F). The patterns of the aged specimens at 893°C (1640°F) were compared with fresh foil heated directly to 893°C (1640°F) (no prolonged high temperature treatment). These results are presented and discussed later.

High Aluminum Foil.-The intensity of the superlattice lines of R 449 was much stronger than R 334 and no interference of the (100) superlattice line with oxides was encountered. The as-received foils could, therefore, be heated directly to the exposure temperatures, 900°C (1652°F), 1000°C (1832°F), and 1073°C (1963°F), without prior grain coarsening treatments. Integrated intensities of the three patterns were measured. These results are discussed later.

Ambient Temperature X-Ray Diffraction

Various X-ray diffraction techniques at 70° ± 2°F were used in this research. Superlattice line measurements of quenched samples were obtained with a self-focusing camera. Minor phases present in the alloys were studied. The foils, used as specimens for elevated temperature X-ray diffraction, were analysed for oxides and preferred orientation. Lattice parameters were measured for compositions used in the investigation of mechanical properties.

Quenched Samples.--Quenched specimens were evaluated structurally in a self-focussing X-ray camera with unfiltered chromium radiation. The exposure time was approximately eight hours.

Minor Phases.--Identification of minor phases was performed for specimens of heats R 332 and 333 after aging at 850°C (1652°F) for 24 hours. The minor phases were extracted by a bromine-anhydrous methyl alcohol solution. The solution plus residue were centrifuged to separate the minor phases. X-ray diffraction patterns, using vanadium-filtered chromium radiation, identified the oxides of nickel, chromium, and aluminum which were apparently embedded into the metal during hot rolling. The data are presented in Table V.

Foils.--The oxides, which formed on the foils used as specimens for elevated temperature X-ray diffraction, were identified by exposure of foil slivers in conventional Debye-Scherrer powder cameras. Vanadium-filtered chromium radiation was used. An exposure of six hours was necessary to make the weak oxide lines visible.

Chromium oxide, Cr_2O_3, predominated at high chromium levels, R 332 and 333 - aluminum oxide, αAl_2O_3, at higher aluminum contents, R 449. Mixtures of both oxides appeared at intermediate analyses. No spinels of nickel and chromium or nickel and aluminum oxides were formed during elevated temperature diffraction. These data are presented in Table VII.

Preferred orientation of the foils was determined by the transmission method using a pinhole camera. The foils were mounted with the rolling direction perpendicular to the incoming beam. As-received and exposed foils were analysed. Unfiltered chromium radiation was used. The exposure time was one-half hour.

All foils used in this research, except R 449, showed preferred orientation. The texture was present in as-received foils (cold-worked)

and foils after exposure (recrystallized). No attempt was made to determine the rolling texture. The absence of preferred orientation in R 449 permitted comparison of theoretical and experimental intensities. Surprisingly, the preferred orientation of heat R 334 did not affect this comparison.

Lattice Parameters.--Lattice parameters of R 436, 437, and 438 were measured to determine whether the phase compositions after final heat treatment at 750°C (1382°F) were identical. The back reflection method was used to determine the lattice parameters.

The specimen filings were prepared on cardboard holders according to a method described by Byrne and Hansen.[48] The lattice constant was computed from measurements of the α_1 and α_2 diffraction lines of planes (420), (331), and (400), using filtered-copper radiation. Cohen's method[49] of least squares was used to calculate the lattice parameters.

The measured lattice parameters are shown in Table VI. Since the range of a_o is only 0.002Å, it is concluded that the phase compositions of the three heats are approximately identical at 750°C (1382°F) for all heat treatments.

Mechanical Properties

The elevated temperature properties were determined from a single phase alloy and two alloys with different γ' dispersions. Some mechanical tests at ambient temperature were performed. Rockwell B hardness measurements were taken of quenched and aged specimens.

Elevated Temperature Properties

Hot tensile and creep-rupture data were obtained from heats R 436, 437, 438, 447, and 448. The elevated temperature strain measurements were made with an extensometer-mirror system with a sensitivity of 0.000005 inch per inch. Since the heating time to reach the correct distribution varied between two and four hours, a uniform time of four hours was used before the stress was applied.

Metallography

Samples for optical and electron microscopy were mounted, ground, and mechanically polished on silicon carbide papers, dry diamond cloths, and wet Linde B cloths. To remove the cold work from these operations, the specimens were polished either automatically on a Syntron with Linde B powder or electrolytically with a 10 percent perchloric-acetic acid solution.

The method of Bigelow, Amy, and Brockway[50] was used to delineate the precipitating phases. Electrolytic etching for 5-10 seconds was usually satisfactory at a current density of 0.5 amperes per square inch. A solution of 12 parts phosphoric acid (85 percent), 45 parts of sulfuric acid (96 percent) and 41 parts of nitric acid (70 percent) was used as the electrolyte.

Light Microscopy

All of the samples prepared in this research were examined by light microscopy. For the most part, the precipitating phase, γ', was too small to resolve at 1000X. Therefore, the use of light microscopy was limited.

The foils exposed in the elevated temperature diffraction camera for longer times developed larger γ' particles and, consequently, were examined mostly by light microscopy. The foils were electroplated with nickel and the cross sections were polished and etched in the usual manner. The structure of the oxide and phases present in the foil were examined at 1000X.

Electron Microscopy

Standard electron microscopy techniques were used in this research. The polished and etched metallic surfaces were replicated with a collodion-amyl acetate solution. Polystyrene latex spheres were placed on the collodion replicas to provide an internal standard for magnification and to indicate the direction of shadowing. The replicas were shadowed with palladium to increase contrast. An RCA Model EML electron microscope was used to examine and photograph the replicated metallic surfaces.

Phases with shadows in the same direction as the polystyrene latex spheres indicate a depression on the original metal surface. Conversely, particles with shadows opposite to those cast by the spheres are protrusions above the metal surface. The electron micrographs are contact prints from the original plates causing the polystyrene spheres to appear black and the "shadows" white.

Quantitative Microstructural Measurements

Two quantitative microstructural measurements were necessary in this research. To correlate the results of the mechanical properties with γ' dispersions, it was necessary to know the average particle size

and planar mean free path. These were calculated from the average particle density and volume percent of γ'. The reproducibility of results was within 10 percent for different areas of the same specimen.

The volume percentage of γ' was determined by superimposing a grid on the electron micrograph and measuring the area of γ' particles in a one-inch square.(51) The particle density was evaluated by counting the number of particles in a one-inch diameter circle. The magnification of the electron micrographs was in general 12,000X which means that the areas sampled were extremely small. However, the γ' precipitation is uniform over the entire sample as guaged by the rather good reproducibility of the measurements.

These quantitative measurements are given in Table IV.

Phase Diagram

The phase studies were concerned initially with the determination of the quasi-binary phase diagram extending from Ni_3Cr to Ni_3Al. This preliminary survey was necessary before proceeding with the investigation of the proposed order-disorder transformation.

The solvus lines determined in this research are shown in Figure 10 and 11. The solubility band shown in Figure 10 was determined from short time heat treatments (12 hours). The equilibrium solvus is shown in Figure 11. The solubility line of Taylor and Floyd is shown in both figures.

The solvus lines determined for short and long time solution-treatments are in fair agreement with the published work of Taylor and Floyd.(1) Differences in solvus temperature of 35 to 100°C occur in the

low aluminum alloys. Minor differences, less than 20°C, in solvus temperature exist at higher aluminum contents. The discrepancies are probably due to differences in chemical analyses. The nickel analyses for the three low aluminum heats prepared in this research are 73, 75.6 and 73.2 atomic percent. The material of Taylor and Floyd was 75, 74.9 and 74.5 atomic percent nickel.

RESULTS AND DISCUSSION

The detailed results and discussion are conveniently presented in the following order: 1) investigation of the order-disorder transformation and 2) the elevated temperature properties of Ni-Cr-Al alloys.

Investigation of the Order-Disorder Transformation

Elevated Temperature X-Ray Diffraction

The elevated temperature X-ray diffraction results indicate that none of the alloys investigated in this research possesses long range ordering based upon Ni_3Cr (Tables VII and VIII and Figures 12 and 13). Table VII contains the details of the diffraction patterns of the materials investigated. Figure 12 summarizes the diffraction results in relation to the equilibrium diagram. Figure 13 shows the theoretically calculated and experimentally determined intensities of heat R 449. Table VIII contains similar data for all alloys investigated.

Before proceeding with the detailed presentation and discussion of the elevated temperature diffraction data, it is necessary to discuss the general interpretation of the patterns. Chromium and aluminum oxide form on the foil surfaces during exposure at temperature. Both oxides were identified in the low aluminum materials, R 332, 333, and 334; only αAl_2O_3 formed on the high aluminum foil, R 449. The 3.63 line of Cr_2O_3 and the 2.55 line at αAl_2O_3 appear extremely close to the positions of the superlattice reflections (3.58-3.60, 2.53-2.55). Therefore, the interpretation of the low aluminum foils was difficult. However, the distinction between oxide and superlattice lines was made by comparing the line appearances and the calculated lattice parameters of the questionable reflections and the main lattice lines.

Theoretically, the superlattice lines and main lattice lines should be similar in appearance. The elevated temperature diffraction research of P. A. Flinn[52] showed that the superlattice lines and main lattice lines were both spotty at higher temperatures where grain growth occurred in the alloy and continuous in fine grained material. In the data of Table VII the lines near the positions of the superlattice reflections were continuous and the main lattice lines spotty for the lower aluminum materials. This indicated that the lines near the possible superlattice reflections were from oxides. Furthermore, the other oxide lines in the elevated temperature diffraction patterns were always continuous.

The interfering oxide lines could also be distinguished from superlattice reflections, in most cases, by their slight difference in d value. This difference, when referred to the a_o of the face-centered alloy lattice is in most instances about 0.06 Å, which is significant. The agreement when superlattice lines are present from the ordered γ' phase is 0.02 Å maximum.

Therefore, if the questionable reflections are continuous and the main lattice lines are spotty, the questionable lines are due to oxides. Also if the lattice parameter calculated from the questionable lines is not in good agreement with the parameters calculated from the main lattice lines, this is additional evidence that the questionable reflections are oxide lines. The details of the elevated temperature diffraction data may now be presented and discussed in the following heat sequence: R 449, 334, and R 333 and R 332 (in order of decreasing Al content.

R 449 (16.1 Atomic Percent Al).--Elevated temperature X-ray diffraction patterns were obtained from heat R 449 at 900°C (1652°F), 1000°C (1832°F), and 1073°C (1963°F). Duplicate patterns were obtained at 1000°C (1832°F) and 1073°C (1963°F), Table VII and Figure 12. All temperatures were within the two phase field, $\gamma + \gamma'$. The integrated intensity ratios of the (100) and (111) are shown in Figure 13 and Table VIII.

The diffraction patterns for all temperatures investigated were similar. Superlattice lines from the ordered γ' phase appeared in all the patterns. The line appearance of the superlattice reflections was identical to the main lattice lines. The lattice parameters from the superlattice reflections and main lattice lines agreed within 0.02 Å.

X-ray diffraction patterns at ambient temperature of small pieces of the foil, which had been used as elevated temperature diffraction specimens, identified the presence of αAl_2O_3 on the foil surface. These patterns were obtained from a conventional Debye-Sherrer powder camera. The pattern of αAl_2O_3 does not interfere with the (100) superlattice reflection. The intensity of the (100) line is therefore representative of the amount of ordered phase. The amount of αAl_2O_3 on the foil surface was apparently very small since the line intensities in the patterns obtained in the Debye-Sherrer camera were weak and were absent from the elevated temperature patterns. The intensity ratio of the (100) reflections (which are only present in ordered material) to the (111) reflection (always present) can therefore, be used as an index of the amount of ordered material.

The experimental integrated intensity ratios of the (100) to the (111) of heat R 449 are shown as a function of temperature in Figure 13.

The experimental values follow the theoretical intensity curves calculated by assuming the only ordered phase present at temperature is γ'. The theoretical intensities, assuming both γ and γ' are ordered, are considerably higher disagreeing with the experimentally determined values.

Therefore, although superlattice lines were present in all these patterns, the integrated intensity ratios indicate that the γ solid solution does not possess long range ordering. The maximum exposure temperature was limited to 1073°C (1963°F) because of vaporization so that the single phase field could not be reached at this aluminum content.

R 334 (12.2 Atomic Percent Al).--Diffraction results from R 334 were obtained at 893°C (1640°F), 982°C (1800°F), and 1038°C (1902°F), Table VII and Figure 12. Two phases, γ and γ' were present at 893°C (1640°F); at 982°C (1800°F) and 1038°C (1902°F) the material was single phase. Duplicate patterns were obtained at 1038°C (1902°F).

Pattern at 893°C.-The elevated temperature diffraction pattern of R 334 at 893°C (1640°F), Film No. 300, contained spotty superlattice lines from the ordered γ' phase; the main lattice lines were also spotty. The calculated lattice parameters of the (100), (110), (111), and (200) diffraction lines agreed within 0.02 Å. In this pattern the spotty reflections of the superlattice and main lattice lines and the lattice parameter calculations identified the ordered γ' phase. Examination of the microstructure of the foil after the exposure corroborated the presence of γ'.

Continuous oxide lines from Cr_2O_3 were also present in the elevated temperature pattern. The presence of Cr_2O_3 was checked by exposing a small piece of the foil, which had been used as the elevated temperature specimen, in a conventional Debye-Sherre powder camera, Film No. 313D. The presence of Cr_2O_3 on the foil surface was confirmed. The Debye pattern also contained lines from αAl_2O_3.

Pattern at 982°C.-The diffraction pattern of R 334 at 982°C (1800°F) contained no superlattice reflections, Film No. 308. Continuous lines occurred near the positions of the superlattice reflections. However, these lines were identified as oxide lines because of their similarity in appearances to other known continuous oxide lines and because of the contrast in comparison with the spotty main lattice reflections. In this one pattern the lattice parameter calculations agreed within 0.02 Å even though the reflections were oxides.

The presence of Cr_2O_3 and αAl_2O_3 was confirmed by exposing a piece of the foil used in Film No. 308 in a conventional Debye-Sherrer powder camera, Film No. 314D.

Pattern at 1038°C.-The elevated temperature diffraction patterns of R 334 at 1038°C (1902°F) contained no superlattice reflections, Films No. 310 and 321. Diffraction lines appeared close to the superlattice reflections but these lines were identified as oxides of Cr_2O_3 and αAl_2O_3. The interfering oxide lines as well as the other oxide lines in the pattern were continuous in comparison with the spotty main lattice lines and the calculated lattice parameters ranged from 3.58 - 3.63 Å, not falling within the agreement of true superlattice reflections.

The patterns of these foils, after cooling rapidly to room temperature from 1038°C (1902°F) in the elevated temperature camera, contained no superlattice reflections, Films No. 311 and 332. The same continuous oxide lines as mentioned previously appeared in this pattern. The calculated lattice parameters ranged from 3.55 Å for the main lattice lines to 3.61 Å for the continuous lines.

The patterns of the foils, which were aged at 893°C (1640°F) after exposure at 1038°C (1902°F) and quenching to room temperature in the camera, contained spotty superlattice reflections from the ordered γ' phase. The foils were aged at 893°C (1640°F) for 24 hours prior to obtaining patterns at this temperature. The spottiness of the superlattice and main lattice lines as well as the agreement in lattice parameter calculations (0.02 Å) identify the lines as superlattice rather than oxide reflections. Other continuous lines in the pattern were identified as oxides of chromium and aluminum. Exposure of small pieces of the foils in a conventional Debye-Sherrer camera after the exposure at 893°C (1640°F) confirmed the presence of γ', Cr_2O_3 and αAl_2O_3.

Integrated intensity ratios of the (100) and (111) reflections for foils heated directly to 893°C (1640°F), Film No. 300, and for foils aged after exposure at 1038°C (1902°F), Films No. 312 and 323, are shown in Table VIII. Since the integrated intensity ratios at 893°C (1640°F) were essentially equivalent regardless of the path of thermal treatment and since the values agree with theoretical computations, it may be concluded that no vaporization occurred during the high temperature exposure at 1038°C (1902°F). Microscopic comparison of foils from Films No. 312, 323, and 300 also showed that no vaporization occurred at 1038°C (1902°F). Figure 14 shows the foil structure after prolonged heating at 893°C (1640°F). The microstructure of foils heated at 1038°C (1902°F) for 72 hours was similar.

The elevated temperature results from heat R 334 indicated that no long range order existed in the γ solid solution at temperature. The patterns of foils quenched from the single phase field indicated that no ordering of the solid solution occurred during quenching to room temperature at this aluminum content.

R 333 and 332 (10.6 and 8.4 Atomic Percent Al Respectively).--Elevated temperature diffraction patterns were obtained from heats R 333 and 332 at 893°C (1640°F), Table VII and Figure 12. At this temperature both compositions were single phase, Figure 15.

The patterns of R 333 and 893°C (1640°F) contained no superlattice reflections, Films No. 289 and 290. Continuous lines appeared near the superlattice reflections but were identified as oxide reflections by comparison of line appearance and lattice parameter calculations. The 2.57 line was absent from Film No. 290. The pattern of the exposed foil, obtained in a Debye-Sherrer camera, showed that the major amount of oxide present was Cr_2O_3 rather than αAl_2O_3, thereby explaining the absence of the 2.57 line in the elevated temperature pattern, Film No. 294D. Most of the oxide lines identified in the Debye-Sherrer pattern appeared in the elevated temperature pattern.

The elevated temperature diffraction pattern of R 332 at 893°C (1640°F) contained no superlattice reflections, Film No. 319. Continuous lines appeared near the positions of the superlattice reflections but were identified as oxide reflections by comparison of line appearance and lattice parameter calculations. The Debye-Sherrer pattern, Film No. 294D, was used as a guide for the oxide identification since the elevated temperature patterns of R 333 and 332 were similar.

The elevated temperature diffraction results obtained from heats R 333 and R 332 indicated that no long range ordering based upon Ni_3Cr, existed in the γ solid solution.

All the elevated temperature diffraction patterns contained some spotty lines that were not identified. The appearance of these spotty lines is different compared with the superlattice and main lattice lines. These reflections are probably from spinels or carbides in the metal foil. Most of the room temperature diffraction patterns of solid samples also contained the same reflections. The minor phases identified from extracts of solid specimens did not define the origin of these lines. None of these lines were near important locations, however.

Ambient Temperature X-Ray Diffraction

Superlattice lines were present in most of the X-ray patterns of specimens quenched from the single phase γ field, Table IX and Figure 16. These superlattice lines were due to γ' precipitation during quenching as shown by the following argument.

The X-ray diffraction patterns of low aluminum alloys (less than 12.2 atomic percent aluminum) quenched from the single phase γ field did not contain superlattice reflections. However, superlattice lines were present in the X-ray patterns of high aluminum alloys (12.2 atomic percent aluminum and greater) quenched from the single phase field. All X-ray patterns of specimens, heat treated in the two phase $\gamma + \gamma'$ field and quenched, contained superlattice reflections from the ordered phase, γ'. The previous discussion (elevated temperature work) showed that the γ phase was neither ordered at temperature nor after quenching to 70°F.

Therefore, the presence of superlattice lines in similar alloys quenched from the single phase field indicates that γ' precipitation occurred during the quenching of solid specimens.

The susceptibility of this system to rapid precipitation was noticed during the phase diagram studies, Figures 17-20. The larger particles of Figures 18 and 19 were present at the heat treating temperature; the smaller particles precipitated during the quenching operation. The particles in specimens quenched from the single phase field, Figures 17 and 20, were difficult to resolve and distinguishing between γ' precipitation and surface roughening was troublesome. To resolve this problem, different specimens from a high aluminum heat, R 380, were quenched from a vertical tube furnace into ice-brine, water, oil and air. Table X contains the measured particle sizes and Figures 21-23 contain photomicrographs of the water, oil, and air-quenched samples. Superlattice lines were present in X-ray patterns of these samples quenched rapidly from the vertical tube furnace. Since the particle size increased with decreasing quenching rate, it was concluded that actual γ' precipitation rather than surface roughening caused the pebbly appearance in the photomicrographs of specimens quenched from the single phase field.

Therefore, the superlattice lines present in high aluminum specimens quenched from the single phase field were due to γ' precipitation. Since no ordering of the γ solid solution was detected, it remained only to consider the role of γ' in affecting properties at elevated temperatures.

Elevated Temperature Properties

Dispersion of γ' particles in the γ solid solution matrix increased the yield strength and creep strength of the wrought Ni-Cr-Al alloys investigated. A corresponding decrease of elongation resulted from γ' precipitation. No significant change in creep strength was measured by varying, by a factor of two, the size and mean free path of the γ' dispersions. The results are shown in Table XI and Figure 24.

The properties obtained from cast test bars were very scattered (probably influenced by shrinkage) and were not representative of the alloys. Therefore, the results from cast material will not be discussed in detail but are included in Table XII.

Effect of the Dispersed γ' Phase

The dispersion of the γ' phase, based upon Ni_3Al, exerts potent effects upon elevated temperature properties. The creep strength [i.e., stress to produce a creep rate of 0.001 percent/hour at 750°C (1382°F)] is five to six times greater for the precipitation hardened material, Figure 24. The yield strength of the two phase alloys is also approximately five to six times that of the single phase alloy, Table XI. The elongation of the single phase material is much greater as would be expected (80-90 percent versus 1-2 percent).

The results are apparently typical of the theoretical effects of precipitation hardening upon elevated temperature properties. Weertman[22] predicts that the creep strength of two phase alloys similar to these would be approximately 10 times that of single phase material.

The intent of this section was to determine the effect of γ' precipitation upon elevated temperature properties and not of simultaneous

changes in phase composition and precipitation. However, the composition of the matrix phase was not exactly equivalent. The preliminary lattice parameter and phase diagram studies indicated that the chemistry of heat R 437 was approximately equal to the composition of the matrix of alloys within the two phase field at 750°C (1382°F), R 436 and R 438. The intended chemistry of the wrought heats used in the property studies, R 447 and R 448, were identical to R 437 and R 436 except for the small boron additions. However, the final analysis of R 447 was enough different from R 437 to result in a change in the composition of the γ solid solution of heats R 447 and 448 when heat treated at 750°C (1382°F). The compositional change is small however, (3-4 atomic percent in Ni, Cr, and Al) and should not materially affect the magnitude of the influence of γ' precipitation upon elevated temperature properties.

Effect of Different Dispersions

Increasing the particle size and mean free path of the γ' precipitate by a factor of two did not significantly affect the creep strength of a typical Ni-Cr-Al alloy (R 448) at 750°C (1382°F) Figures 24, 25, and 26. In view of the dispersion hardening theories of Mott and Nabarro[12] and Orowan[53] a change in creep strength would be expected.

Recently Weertman[22] postulated that particle size as well as mean free path was an important variable in affecting deformation at elevated temperatures. Using Weertman's equations and the values for the dispersions developed in this research, the creep strengths for both dispersions should be essentially equivalent. However, the dispersion change

was not enough different to test Weertman's theory thoroughly. The data, however, show that particle coalescence over the range investigated does not significantly affect the creep strength Ni-Cr-Al alloys.

Fracture

The alloys prepared in this research fractured intergranularly. The steady-state creep rates were measured before any pronounced micro-cracking occurred. No significant changes in the γ' dispersions occurred during elevated temperature testing.

CONCLUSIONS

An experimental study was conducted to investigate the structural transformations present in Ni-Cr-Al alloys and to correlate the transformations with changes in elevated temperature properties. According to the literature two transformations existed: 1) an order-disorder transformation of the γ solid solution, rich in Ni and Cr, and 2) precipitation hardening by an ordered phase based upon Ni_3Al, γ'.

No long range ordering was found in the γ solid solution by elevated temperature X-ray diffraction. Conventional X-ray diffraction patterns of quenched specimens contained superlattice reflections but these reflections resulted from precipitation of the ordered phase, γ' during quenching.

Therefore, the important transformation affecting creep properties in the Ni-Cr-Al system is the precipitation of the ordered phase γ'. This precipitation of γ' particles markedly increases the elevated temperature properties at 750°C (1382°F). The yield strength is increased by a factor of five to six. A 40-fold decrease in percent elongation results from γ' precipitation. The creep strength [i.e., the stress necessary to produce a creep rate of 0.001 percent/hour at 750°C (1382°F)] is increased five to six fold by γ' precipitation. Small changes in the γ' dispersion did not significantly affect the creep strength at 750°C (1382°F).

TABLES I THROUGH XII

TABLE I

INTENDED ANALYSES AND RAW MATERIALS USED IN ALLOY PREPARATION

Heat No.	Intended Analyses						Special Raw Materials and Additions *		
	Wt. %			At. %					
	Ni	Cr	Al	Ni	Cr	Al	Material	Purity	Special Additions
R 332	78.3	18.8	2.9	75	20	5	electrolytic Cr	99.9 % Cr	none
R 333	80.1	14.5	5.4	75	15	10	"	"	"
R 334	79.7	15.4	4.9	75	16	9	"	"	"
R 379	82.23	10.7	7.07	75	11	14	"	"	"
R 380	83.0	8.84	8.16	75	9	16	"	"	"
R 346	83.0	8.84	8.16	75	9	16	"	"	"
R 347	84.6	5.0	10.4	75	5	20	"	"	"
R 436	80.4	15.21	4.44	75	16	9	low carbon high purity Cr	99.96% Cr 0.008% C	"
R 437	78.2	20.35	1.45	75	22	3	"	"	"
R 438	82.6	9.76	7.61	75	10	15	"	"	"
R 447	78.2	20.35	1.45	75	22	3	shield alloy	99.4 % Cr 0.05% C	90 ppm Boron
R 448	80.4	15.21	4.44	75	16	9	"	"	"
R 449	80.1	14.5	5.4	75	10	15	electrolytic Cr	99.9 % Cr	none

* Electrolytic nickel (99.97%) and high purity aluminum piglets (99.99%) were the other raw materials.

TABLE II

CHEMICAL ANALYSES OF Ni-Cr-Al ALLOYS

Heat No.	Aim Analyses		Final Analyses									
	Atomic %*		Weight %							Atomic %		
	Cr	Al	Ni	Cr	Al	C	N	B	Zr	Ni	Cr	Al
R 332	20	5	77.87	17.51	4.14	0.03	0.0126	-	< 0.01	73	18.6	8.4
R 333	15	10	81.42	13.08	5.25	0.03	0.0098	-	"	75.6	13.7	10.6
R 334	16	9	79.62	14.11	6.15	0.05	0.0084	-	"	73.2	14.6	12.2
R 379	11	14	82.05	10.09	7.65	0.05	0.0075	-	"	74.5	10.4	15.1
R 380	9	16	82.40	8.63	8.70	0.04	0.0125	-	"	74.2	8.8	17.0
R 346	9	16	82.96	8.04	8.83	0.07	0.007	-	"	74.6	8.2	17.2
R 347	5	20	85.92	4.22	9.93	0.04	0.007	-	"	76.5	4.3	19.2
R 436	16	9	79.66	14.79	5.33	-	0.0084	-	-	73.8	15.4	10.75
R 437	22	3	77.89	19.49	2.48	-	0.0056	-	-	73.8	20.9	5.12
R 438	10	15	82.20	9.53	8.03	-	0.0070	-	-	74.5	9.74	15.85
R 447	22	3	82.53	15.72	1.64	0.005	0.003	0.0032	-	79.6	17.0	3.4
R 448	16	9	80.49	14.82	4.63	0.0062	0.002	0.0055	-	75.0	15.6	9.4
R 449	10	15	78.88	12.64	8.23	0.02	-	-	-	71	12.9	16.1

* Balance nickel.

TABLE III

HEAT TREATMENTS, HARDNESS, AND STRUCTURES OF SAMPLES
FOR PHASE DIAGRAM AND QUENCHED X-RAY STUDIES

Heat and Spec. No.(1)	Temp °C	Time hr.	R_B Hardness 95% Conf. Limits	Structures(5)
R 332 - 90w	705	24	-	$\gamma + \gamma'$
- 158w(6)	750	24	-	$\gamma + \gamma'$
- 157w(6)	850	24	-	No visible γ' particles
- 91w(6)	1000	12	72.2 ± 2.2	" " " "
- 92w	1200	12	61.7 ± 0.5	" " " "
- 137w	754	504	-	$\gamma + \gamma'$
- 121w	800	500	63.1 ± 1.3	No visible γ' particles
- 113w	849	168	75.0 ± 1.0	" " " "
- 111w	900	168	75.4 ± 0.5	" " " "
R 333 - 160w(6)	750	24	-	$\gamma + \gamma'$
- 93w(6)	850	12	87.9 ± 1	$\gamma + \gamma'$
- 134w	875	24	-	$\gamma + \gamma'$
- 39c	900	25.5	-	$\gamma + \gamma'$
- 124w	900	24	-	No visible γ' particles
- 133w	934	24	71.2 ± 1.5	" " " "
- 159w(6)	950	24	-	" " " "
- 38c	1000	12	54.2 ± 2.2	" " " "
- 119a	1000	12	56.0 ± 2.2	" " " "
- 135a(2)	1000	12	60.0 ± 1.0	" " " "
- 134a(3)	1000	12	71.9 ± 1.8	" " " "
- 120 (4)	1000	12	74.8 ± 1.5	" " " "
- 94w(6)	1076	12	-	" " " "
- 74c	1087	12	61.9 ± 2.2	" " " "
- 95w	1206	12	-	" " " "
- 120w	854	165	-	$\gamma + \gamma'$
- 138w	854	505	-	$\gamma + \gamma'$
- 119w	904	168	-	No visible γ' particles
- 110c	954	168	56.2 ± 1.5	" " " "
- 107c	1004	168	56.7 ± 2.2	" " " "
R 334 - 96w(6)	850	24	-	$\gamma + \gamma'$
- 87w	900	24	-	$\gamma + \gamma'$
- 44c	900	25.5	-	$\gamma + \gamma'$
- 24c	950	24	-	$\gamma + \gamma'$
- 43c	1000	11.5	-	$\gamma + \gamma'$
- 142w	1000	12	-	No visible γ' particles
- 130w	1029	12	82.6 ± 0.5	" " " "
- 73c	1040	12	-	" " " "
- 18c	1054	12	-	" " " "
- 97c(6)	1076	12	96.1 ± 1.5	" " " "
- 72c	1149	11.5	-	" " " "
- 98w	1206	12	83.1 ± 1.8	" " " "
- 118c	904	168	-	$\gamma + \gamma'$
- 139w	910	505	-	$\gamma + \gamma'$
- 109c	950	168	70.4 ± 1.5	No visible γ' particles
- 79c	1000	170	-	" " " "
R 379 - 171w(6)	750	24	-	$\gamma + \gamma'$
- 49c	900	25.5	-	$\gamma + \gamma'$
- 48c	950	23.5	-	$\gamma + \gamma'$
- 46c	1000	11.5	-	$\gamma + \gamma'$
- 108w(6)	1004	13.5	-	$\gamma + \gamma'$
- 154w	1072	12	-	$\gamma + \gamma'$
- 47c	1100	12	-	$\gamma + \gamma'$
- 143c	1110	12.5	94.8 ± 1.5	γ + visible γ' particles ppt'd during quench
- 136w	1132	14	-	" " " "
- 147w(6)	1150	12	98.3 ± 2	" " " "
- 100w	1172	12	-	" " " "
- 69c	1200	12	87.2 ± 2	" " " "
- 70c	1090	168	-	$\gamma + \gamma'$
- 104c	1149	168	92.2 + 0.3	No visible γ' particles

TABLE III (CONT'D)

HEAT TREATMENTS, HARDNESS, AND STRUCTURES OF SAMPLES
FOR PHASE DIAGRAM AND QUENCHED X-RAY STUDIES

Heat and Spec. No.(1)	Temp. °C	Time hr.	R_B Hardness 95% Conf. Limits	Structures(5)
R 380 - 55c	950	23.5	-	$\gamma + \gamma'$
- 53c	1000	11.5	-	$\gamma + \gamma'$
- 52c	1062	12.0	-	$\gamma + \gamma'$
- 54c	1100	12	-	$\gamma + \gamma'$
- 57c	1200	11.5	-	γ + visible γ' particles ppt'd during quench
- 225w(6)	1200	12	-	" " " "
- 226w(2,6)	1200	12	-	" " " "
- 227w(3,6)	1200	12	93.0 ± 1.5	" " " "
- 228w(4,6)	1200	12	98.3 ± 0.8	" " " "
R 346 - 22c	950	24	-	$\gamma + \gamma'$
- 85w(6)	998	12	-	$\gamma + \gamma'$
- 42c	1000	11.5	-	$\gamma + \gamma'$
- 62c	1040	12	-	$\gamma + \gamma'$
- 41c	1062	12	-	$\gamma + \gamma'$
- 68w(6)	1093	12	-	$\gamma + \gamma'$
- 16c	1095	12	-	$\gamma + \gamma'$
- 64c	1149	11.5	-	γ and visible γ' particles ppt'd during quench
- 62w	1149	11.5	-	$\gamma + \gamma'$
- 12c	1148	12	-	γ + visible γ' particles ppt'd during quench
- 131w	1185	12	92.8 ± 1.5	" " " "
- 84w(6)	1193	12	-	" " " "
- 8c	1200	12	-	" " " "
- 61c	1200	11.5	94.6 ± 1.5	" " " "
- 63c	1262	14	-	" " " "
- 105c	1090	168	-	$\gamma + \gamma'$
- 103c	1149	168	-	No visible γ' particles
R 347 - 82a(6)	750	24	-	$\gamma + \gamma'$
- 20c	954	24	-	$\gamma + \gamma'$
- 36c	1000	12	-	$\gamma + \gamma'$
- 66a(6)	1000	12	-	$\gamma + \gamma'$
- 35c	1062	12	-	$\gamma + \gamma'$
- 14c	1095	12	-	$\gamma + \gamma'$
- 83w(6)	1098	12	-	$\gamma + \gamma'$
- 10c	1148	12	-	$\gamma + \gamma'$
- 151c	1171	12	-	γ and visible γ' particles ppt'd during quench
- 132w	1185	12	-	$\gamma + \gamma'$
- 65c	1200	11.5	-	γ + visible γ' particles ppt'd during quench
- 66w(6)	1200	11.5	-	" " " "
- 76c	1204	17	-	" " " "
- 77c	1143	169	-	$\gamma + \gamma'$
- 102c	1149	168	88.5 ± 2.0	γ and visible γ' particles
- 99c	1177	168	90.6 ± 1.5	ppt'd during quench

(1) All specimens were quenched in ice-brine from temperature unless noted. As-cast and wrought samples are designated by c or w after the sample number. As-cast samples were homogenized at 1200°C (2200°F) - four hours before treatments. Wrought samples were heat treated directly from hot-rolled condition.

(2) Water quenched from temperature.

(3) Oil quenched from temperature.

(4) Air quenched from temperature.

(5) Structures were examined at 12,000X and higher magnifications.

(6) Sample used in quenched X-ray studies.

TABLE IV

HEAT TREATMENTS FOR SPECIMENS AND TEST BARS FOR MECHANICAL TESTING

Heat and Specimen No.(1)	Aging Temp. °C	Time hr.	R_B Hardness	Structures	Vol. % γ'	Avg. Particle Size Å	Planar Mean Free Path (cm.)
			Cast Specimens and Test Bars				
R 436 - 165	as quenched	0	84.2 ± 1.5	$\gamma + \gamma'$			
- 166	750	4	-	$\gamma + \gamma'$			
- 167	750	8	98.7 ± 0.5	$\gamma + \gamma'$			
- 168	750	24	99.5 ± 0.5	$\gamma + \gamma'$			
- 169	750	100	100.4 ± 0.8	$\gamma + \gamma'$	32.8	577	1.34×10^{-5}
- 170	750	300	102.5 ± 0.8	$\gamma + \gamma'$	36.6	619	-
R 436 - 195	871	24					
	Furnaced cooled to 750°C						
	750	24		$\gamma + \gamma'$	32.6	1240	2.89×10^{-5}
R 437 - 191	750	24	56.8 ± 1.5	No visible γ'	0		
R 438 - 175	750	4	95.7 ± 0.8	$\gamma + \gamma'$			
- 174	750	8	96.5 ± 0.8	$\gamma + \gamma'$			
- 173	750	24	97.9 ± 1.0	$\gamma + \gamma'$			
- 176	750	100	101 ± 0.3	$\gamma + \gamma'$			
- 177	750	300	99.6 ± 0.8	$\gamma + \gamma'$			
R 436 - 1,6, 7,8*	750	100	98.7 ± 0.5	$\gamma + \gamma'$			
R 437 - 3,4, 6,7,8*	750	24	77.3 ± 2.0	No visible γ'	0		
R 438 - 4,5*	954	24	99.8 ± 1.0				
	Furnaced cooled 750°C						
	750	24		$\gamma + \gamma'$			
			Wrought Specimens and Test Bars				
R 447 - 1(2) thru 8*	750	24	64.5 ± 1.3	No visible γ'	0		
R 448 - 1,2,(2) 3,8*	871	24					
	Furnace cooled to 750°C						
	750	24	103.3 ± 0.5	$\gamma + \gamma'$	39.8	1200	2.15×10^{-5}
R 448 - 4,5,(2) 6,7*	750	100	102. ± 0.5	$\gamma + \gamma'$	41.0	655	1.15×10^{-5}

(1) Samples were homogenized and solution-treated at 1200°C (2192°F) for 24 hours unless otherwise noted. All test bars were air-cooled from temperature unless otherwise noted.

(2) Solution-treated at 1000°C (1832°F) for 12 hours.

* Test bars, R 436, 437, and 438 cast, R 447 and R 448 wrought.

TABLE V

X-RAY DIFFRACTION PATTERNS OF MINOR PHASES EXTRACTED FROM HEATS R 332 AND R 333 AFTER AGING AT 850°C (1562°F) FOR 24 HOURS

d Range	Pattern of R 332-157			Pattern of R 333-159		
	d	I	Ident.	d	I	Ident.
3.50 - 3.60	3.60	70	Cr_2O_3	3.60	30	Cr_2O_3
2.70 - 3.49	3.45	30	Al_2O_3			
2.60 - 2.69	2.66	80	Cr_2O_3	2.67	30	Cr_2O_3
2.50 - 2.59	2.55	70	Al_2O_3			
2.40 - 2.49	2.47	80	Cr_2O_3	2.48 2.42	30 90	Cr_2O_3 NiO
2.30 - 2.39	2.36	60	Al_2O_3			
2.20 - 2.29	2.28	70	-	2.29	20	-
2.10 - 2.19	2.17 2.10	70 80	Cr_2O_3 Al_2O_3			
2.00 - 2.09	2.04	20	Cr_2O_3	2.09	90	NiO
1.90 - 1.99						
1.80 - 1.89	1.81	60	Cr_2O_3			
1.70 - 1.79	1.74	60	Al_2O_3			
1.65 - 1.69	1.67	80	Cr_2O_3	1.67	30	Cr_2O_3
1.60 - 1.64	1.62 1.60	70 80	Cr_2O_3 Al_2O_3	1.62	30	Cr_2O_3
1.55 - 1.59	1.58	20	Cr_2O_3			
1.50 - 1.54	1.52	20	Al_2O_3			
1.45 - 1.49	1.46	80	Cr_2O_3	1.48	90	NiO
1.40 - 1.44	1.43 1.41	80 80	Cr_2O_3 Al_2O_3	1.43	30	Cr_2O_3
1.35 - 1.39	1.38 1.37	70 90	Al_2O_3	1.38	30	-
1.30 - 1.34	1.32	70	-			
1.25 - 1.29	1.295	70	Cr_2O_3	1.26	90	NiO
1.20 - 1.24	1.24 1.21	90 60	Al_2O_3 Cr_2O_3	1.21	90	NiO
1.15 - 1.19	1.19	60	Cr_2O_3			

TABLE VI

LATTICE PARAMETERS, AFTER THE FINAL AGING TREATMENT AT 750°C (1382°F), OF MATERIAL USED FOR MECHANICAL TESTING

Heat No.	Lattice Parameter, Å *	Description of Line Profile
R 437 - 191	3.554_1	sharp
R 436 - 169	3.555_5	diffuse
R 436 - 195	3.555_8	diffuse
R 438 - 172	3.556_6	sharp

* Ambient Temperature: 70° ± 2°F

TABLE VII

ELEVATED TEMPERATURE X-RAY DIFFRACTION PATTERNS

Heat No.	Film[1] No.	Temp.[2] °C	d Range	Pattern at Temperature				Quenched Pattern				Aged Patterns				Pattern of Foil Sliver Exposed in Debye-Sherrer Powder Camera			
				d(3)	I(4)	a_o(5)	Ident.(6)	d(3)	I(4)	a_o(5)	Ident.(6)	d(3)	I(4)	a_o(5)	Ident.(6)	d(3)	I(4)	a_o(5)	Ident.(6)
R 332	319	893	3.90 - > 4.0				-												
			3.80 - 3.89	3.82	30 sp														
			3.70 - 3.79																
			3.60 - 3.69	3.63	10	3.63	Cr_2O_3												
			3.50 - 3.59																
			3.40 - 3.49	3.49	10		Al_2O_3												
			3.30 - 3.39																
			3.20 - 3.29	3.25	30 sp		-												
			3.10 - 3.19	3.13	20 sp		-												
			3.00 - 3.09																
			2.70 - 2.99	2.70	20		Cr_2O_3												
			2.60 - 2.69																
			2.50 - 2.59	2.55	20	3.60	Al_2O_3												
			2.40 - 2.49	2.48	20		Cr_2O_3												
			2.30 - 2.39																
			2.20 - 2.29																
			2.10 - 2.19																
			2.00 - 2.09	2.07	90 sp	3.59	γ												
			1.80 - 1.99																
			1.70 - 1.79	1.79	80 sp	3.58	γ												
			1.60 - 1.69																
			1.50 - 1.59																
			1.40 - 1.49																
			1.30 - 1.39																
			1.20 - 1.29																
			1.10 - 1.19																
R 333	289	893	3.90 - > 4.0																
			3.80 - 3.89	3.82	30 sp		-												
			3.70 - 3.79																
			3.60 - 3.69	3.62	70	3.62	Cr_2O_3												
			3.50 - 3.59	3.51	30		Al_2O_3												
			3.40 - 3.49																
			3.30 - 3.39																
			3.20 - 3.29	3.25	60 sp		-												
			3.10 - 3.19																
			3.00 - 3.09																
			2.70 - 2.99	2.70	70		Cr_2O_3												
			2.60 - 2.69																
			2.50 - 2.59	2.57	30	3.63	Al_2O_3												
			2.40 - 2.49	2.49	70		Cr_2O_3												
				2.42	20		Al_2O_3												
			2.30 - 2.39																
			2.20 - 2.29																
			2.10 - 2.19																
			2.00 - 2.09	2.08	100 sp	3.60	γ												
			1.80 - 1.99																
			1.70 - 1.79	1.79	90 sp	3.58	γ												
			1.60 - 1.69																
			1.50 - 1.59																
			1.40 - 1.49																
			1.30 - 1.39																
			1.20 - 1.29																
			1.10 - 1.19																
R 333	290	893	3.90 - > 4.0																
	294D		3.80 - 3.89	3.81	60 sp		-												
			3.70 - 3.79																
			3.60 - 3.69	3.63	60	3.63	Cr_2O_3									3.63	60	3.63	Cr_2O_3
			3.50 - 3.59																
			3.40 - 3.49	3.49	20		Al_2O_3												
			3.30 - 3.39																
			3.20 - 3.29	3.25	60 sp		-												
			3.10 - 3.19																
			3.00 - 3.09																
			2.70 - 2.99																
			2.60 - 2.69	2.68	60		Cr_2O_3									2.66	60		Cr_2O_3
			2.50 - 2.59													2.56	30	3.62	Al_2O_3
			2.40 - 2.49	2.49	60		Cr_2O_3									2.48	60		Cr_2O_3
			2.30 - 2.39																
			2.20 - 2.29																
			2.10 - 2.19													2.17	30		Cr_2O_3
			2.00 - 2.09	2.07	100 sp	3.59	γ									2.05	100	3.55	γ
			1.80 - 1.99													1.82	30		Cr_2O_3
			1.70 - 1.79	1.79	90 sp	3.58	γ									1.77	100	3.54	γ
			1.60 - 1.69													1.67	60		Cr_2O_3
																1.60	60		Cr_2O_3 + Al_2O_3
			1.50 - 1.59																
			1.40 - 1.49													1.46	60		Cr_2O_3
																1.43	60		Cr_2O_3
			1.30 - 1.39													1.375	30		Al_2O_3
			1.20 - 1.29													1.295	30		Cr_2O_3
																1.26	30		Cr_2O_3
			1.10 - 1.19																

TABLE VII (CONT'D)

ELEVATED TEMPERATURE X-RAY DIFFRACTION PATTERNS

Heat No.	Film[1] No.	Temp.[2] °C	d Range	Pattern at Temperature				Quenched Pattern				Aged Pattern				Pattern of Foil Sliver Exposed in Debye-Sherrer Powder Camera			
				d[3]	I[4]	a_o[5]	Ident.[6]	d[3]	I[4]	a_o[5]	Ident.[6]	d[3]	I[4]	a_o[5]	Ident.[6]	d[3]	I[4]	a_o[5]	Ident.[6]
R 334	300	893	3.90 - > 4.0	4.34	10		-												
	313C		3.80 - 3.89	3.81	20 sp		-												
			3.70 - 3.79													3.78	20		—
			3.60 - 3.69																
			3.50 - 3.59	3.59	30 sp	3.59	γ'									3.55	20	3.55	γ'
			3.40 - 3.49																
			3.30 - 3.39																
			3.20 - 3.29	3.24	20		-												
			3.10 - 3.19																
			3.00 - 3.09																
			2.70 - 2.99																
			2.60 - 2.69	2.67	20		Cr_2O_3									2.68	20		Cr_2O_3
			2.50 - 2.59	2.54	30 sp	3.59	γ'									2.55	20	3.60	Al_2O_3
			2.40 - 2.49	2.49	20		Cr_2O_3												
			2.30 - 2.39																
			2.20 - 2.29																
			2.10 - 2.19																
			2.00 - 2.09	2.065	90 sp	3.58	γ + γ'									2.06	90 sp	3.57	γ + γ'
			1.80 - 1.99																
			1.70 - 1.79	1.785	80 sp	3.57	γ + γ'									1.78	80 sp	3.56	γ + γ'
			1.60 - 1.69													1.68	20		Cr_2O_3
																1.61	20		Cr_2O_3 + Al_2O_3
			1.50 - 1.59																
			1.40 - 1.49																
			1.30 - 1.39																
			1.20 - 1.29													1.26	90 sp	3.56	γ + γ'
			1.10 - 1.19													1.185	20		Cr_2O_3
R 334	308	982	3.90 - > 4.0	4.28	10		-												
	314D		3.80 - 3.89	3.81	30 sp		-												
			3.70 - 3.79																
			3.60 - 3.69	3.60	30	3.60	Cr_2O_3												
			3.50 - 3.59																
			3.40 - 3.49	3.47	20		Al_2O_3												
			3.30 - 3.39																
			3.20 - 3.29	3.24	30		-												
			3.10 - 3.19																
			3.00 - 3.09																
			2.70 - 2.99	2.70	20		Cr_2O_3									2.72	30		Cr_2O_3
			2.60 - 2.69																
			2.50 - 2.59	2.54	30	3.59	Al_2O_3									2.56	30		Al_2O_3
			2.40 - 2.49	2.49	30		Cr_2O_3												
			2.30 - 2.39																
			2.20 - 2.29																
			2.10 - 2.19																
			2.00 - 2.09	2.07	100 sp	3.59	γ									2.06	90 sp	3.57	γ
			1.80 - 1.99																
			1.70 - 1.79	1.79	90 sp	3.58	γ									1.78	80 sp	3.56	γ
			1.60 - 1.69													1.69	20		Cr_2O_3
																1.61	20		Cr_2O_3 + Al_2O_3
			1.50 - 1.59																
			1.40 - 1.49																
			1.30 - 1.39																
			1.20 - 1.29													1.26	90 sp		γ
																1.25	30		Cr_2O_3 + Al_2O_3
			1.10 - 1.19																
R 334	310	1038	3.90 - > 4.0									4.31	20	-	-				
	311Q	R.T.	3.80 - 3.89	3.82	30 sp		-												
	312A	893	3.70 - 3.79					3.79	30 sp		-	3.79	30 sp	-	-				
	320D		3.60 - 3.69	3.63	20	3.63	Cr_2O_3	3.61	10	3.61	Cr_2O_3								
			3.50 - 3.59									3.58	50 sp	3.58	γ'	3.59	30	3.59	γ'
			3.40 - 3.49	3.47	20		Al_2O_3	3.45	20		Al_2O_3	3.47	30		Al_2O_3				
			3.30 - 3.39																
			3.20 - 3.29	3.24	30 sp		-	3.22	30 sp		-	3.23	50 sp		-				
			3.10 - 3.19	3.10	20		-					3.11	20 sp		-				
			3.00 - 3.09					3.08	20 sp		-					3.05	20		—
			2.70 - 2.99																
			2.60 - 2.69	2.65	20		Cr_2O_3					2.65	20		Cr_2O_3	2.58	30		Cr_2O_3
			2.50 - 2.59	2.55	30	3.60	Al_2O_3	2.54	30	3.60	Al_2O_3	2.54	70 sp	3.59	γ'	2.52	30	3.58	γ'
			2.40 - 2.49	2.49	30		Cr_2O_3	2.46	20		Cr_2O_3	2.47	50		Cr_2O_3				
			2.30 - 2.39	2.39	30		Al_2O_3	2.38	20		Al_2O_3	2.39	30		Al_2O_3				
			2.20 - 2.29																
			2.10 - 2.19																
			2.00 - 2.09	2.07	90 sp	3.59	γ					2.07	100 sp	3.59	γ + γ'				
				2.05	50		Al_2O_3 Cr_2O_3	2.05	90 sp	3.55	γ	2.05	50		Cr_2O_3	2.06	90 sp	3.57	γ + γ'
			1.80 - 1.99																
			1.70 - 1.79	1.79	80 sp	3.58	γ	1.775	80 sp	3.55	γ	1.79	90 sp	3.56	γ + γ'	1.78	80 sp	3.56	γ + γ'
												1.77	20		Al_2O_3				
			1.60 - 1.69													1.60	20		γ'
			1.50 - 1.59													1.57	20		Cr_2O_3
			1.40 - 1.49													1.46	10		γ'
			1.30 - 1.39													1.37	10		Al_2O_3
			1.20 - 1.29													1.29	20		Cr_2O_3
																1.26	90 sp	3.56	γ + γ'
			1.10 - 1.19													1.24	30		Cr_2O_3

TABLE VII (CONT'D)

ELEVATED TEMPERATURE X-RAY DIFFRACTION PATTERNS

Heat No.	Film[1] No.	Temp.[2] °C	d Range	Pattern at Temperature				Quenched Pattern				Aged Pattern				Pattern of Foil Silver Exposed in Debye-Sherrer Powder Camera			
				d[3]	I[4]	a_o[5]	Ident.[6]	d[3]	I[4]	a_o[5]	Ident.[6]	d[3]	I[4]	a_o[5]	Ident.[6]	d[3]	I[4]	a_o[5]	Ident.[6]
R 334	321	1038	3.90 - > 4.0					4.26	30 sp		-								
	322Q	R.T.	3.80 - 3.89	3.82	20 sp		-												
	323A	893	3.70 - 3.79					3.74	60 sp		-	3.79	30 sp		-				
			3.60 - 3.69	3.63	10	3.63	Cr_2O_3	3.61	10	3.61	Cr_2O_3								
			3.50 - 3.59									3.59	30 sp	3.59	γ'				
			3.40 - 3.49	3.49	30		Al_2O_3	3.46	30		Al_2O_3	3.48	80		Al_2O_3				
			3.30 - 3.39																
			3.20 - 3.29	3.25	30 sp		-	3.20	50 sp		-	3.25	30 sp		-				
			3.10 - 3.19					3.14	20		-								
			3.00 - 3.09																
			2.70 - 2.99																
			2.60 - 2.69	2.67	20		Cr_2O_3												
			2.50 - 2.59	2.56	20	3.62	Al_2O_3	2.54	30	3.60	Al_2O_3	2.54	50 sp	3.59	γ - Al_2O_3				
			2.40 - 2.49	2.49	20		Cr_2O_3	2.45	30		Cr_2O_3	2.46	30		Cr_2O_3				
			2.30 - 2.39	2.39	20		Al_2O_3	2.38	30		Al_2O_3	2.38	30		Al_2O_3				
			2.20 - 2.29																
			2.10 - 2.19																
			2.00 - 2.09	2.08	90 sp	3.60	γ	2.05	100 sp	3.55	γ	2.065	90 sp	3.58	γ + γ'				
			1.80 - 1.99	1.80	80 sp	3.61	γ												
			1.70 - 1.79					1.775	90 sp	3.55	γ	1.785	80 sp	3.57	γ + γ'				
			1.60 - 1.69																
			1.50 - 1.59																
			1.40 - 1.49																
			1.30 - 1.39																
			1.20 - 1.29																
			1.10 - 1.19																
R 449	267	900	3.90 - > 4.0	4.14	10		-	4.26	20		-								
	269Q	R.T.						4.07	10		-								
			3.80 - 3.89	3.81	20 sp		-												
			3.70 - 3.79					3.76	20		-								
			3.60 - 3.69																
			3.50 - 3.59	3.58	70 sp	3.58	γ'	3.56	70 sp	3.56	γ'								
			3.40 - 3.49					3.44	20 sp		-								
			3.30 - 3.39																
			3.20 - 3.29	3.26	20 sp		-												
			3.10 - 3.19																
			3.00 - 3.09					3.07	10		-								
			2.70 - 2.99																
			2.60 - 2.69																
			2.50 - 2.59	2.53	70 sp	3.58	γ'	2.52	70 sp	3.56	γ'								
			2.40 - 2.49																
			2.30 - 2.39																
			2.20 - 2.29																
			2.10 - 2.19																
			2.00 - 2.09	2.07	80 sp	3.59	γ + γ'	2.06	80 sp	3.57	γ + γ'								
			1.80 - 1.99																
			1.70 - 1.79	1.79	70 sp	3.58	γ + γ'	1.775	70 sp	3.55	γ + γ'								
			1.60 - 1.69																
			1.50 - 1.59																
			1.40 - 1.49																
			1.30 - 1.39																
			1.20 - 1.29																
			1.10 - 1.19																
R 449	270	1000	3.90 - > 4.0																
	271	1000	3.80 - 3.89	3.81	20		-												
	315D		3.70 - 3.79																
			3.60 - 3.69																
			3.50 - 3.59	3.59	30	3.59	γ'									3.51	20		Al_2O_3
			3.40 - 3.49																
			3.30 - 3.39																
			3.20 - 3.29	3.26	20		-												
			3.10 - 3.19																
			3.00 - 3.09	3.05	10		-												
			2.70 - 2.99																
			2.60 - 2.69																
			2.50 - 2.59	2.55	30	3.60	γ'									2.53	30	3.58	Al_2O_3
			2.40 - 2.49																
			2.30 - 2.39																
			2.20 - 2.29																
			2.10 - 2.19																
			2.00 - 2.09	2.08	80	3.60	γ + γ'									2.06	90	3.57	γ
			1.80 - 1.99																
			1.70 - 1.79	1.795	70	3.59	γ + γ'									1.78	80	3.56	γ
			1.60 - 1.69													1.60	20		Al_2O_3
			1.50 - 1.59																
			1.40 - 1.49													1.43	20		Al_2O_3
			1.30 - 1.39																
			1.20 - 1.29													1.26	90	3.56	γ
			1.10 - 1.19													1.185	30		Al_2O_3

TABLE VII (CONT'D)

ELEVATED TEMPERATURE X-RAY DIFFRACTION PATTERNS

Heat No.	Film[1] No.	Temp.[2] °C	d Range	Pattern at Temperature				Quenched Pattern				Aged Pattern				Pattern of Foil Sliver Exposed in Debye-Sherrer Powder Camera			
				d[3]	I[4]	a_o[5]	Ident.[6]	d[3]	I[4]	a_o[5]	Ident.[6]	d[3]	I[4]	a_o[5]	Ident.[6]	d[3]	I[4]	a_o[5]	Ident.[6]
R 449	296	1000	3.90 - > 4.0	4.15	10		=												
	316D		3.80 - 3.89	3.81	30 sp		=												
			3.70 - 3.79																
			3.60 - 3.69																
			3.50 - 3.59	3.59	60	3.59	γ'									3.51	20		Al_2O_3
			3.40 - 3.49																
			3.30 - 3.39																
			3.20 - 3.29	3.26	30		-												
			3.10 - 3.19	3.11	20		-												
			3.00 - 3.09																
			2.70 - 2.99																
			2.60 - 2.69	2.67	10		Cr_2O_3												
			2.50 - 2.59	2.54	60	3.59	γ'									2.53	20	3.58	Al_2O_3
			2.40 - 2.49																
			2.30 - 2.39																
			2.20 - 2.29																
			2.10 - 2.19																
			2.00 - 2.09	2.08	90	3.60	γ + γ'									2.065	90	3.58	γ
			1.80 - 1.99																
			1.70 - 1.79	1.795	80	3.59	γ + γ'									1.785	80	3.58	γ
			1.60 - 1.69													1.625	10		—
			1.50 - 1.59													1.59	20		Al_2O_3
			1.40 - 1.49																
			1.30 - 1.39																
			1.20 - 1.29													1.26	90	3.56	γ
			1.10 - 1.19																
R 449	284	1073	3.90 - > 4.0																
	328	1073	3.80 - 3.89	3.84	30		-												
	317D		3.70 - 3.79																
			3.60 - 3.69	3.63	70	3.63	γ'												
			3.50 - 3.59													3.53	30		Al_2O_3
			3.40 - 3.49																
			3.30 - 3.39																
			3.20 - 3.29	3.29	30		-												
			3.10 - 3.19	3.15	30		-												
			3.00 - 3.09																
			2.70 - 2.99																
			2.60 - 2.69																
			2.50 - 2.59	2.56	70	3.62	γ'									2.56	50		Al_2O_3
			2.40 - 2.49																
			2.30 - 2.39																
			2.20 - 2.29																
			2.10 - 2.19	2.10	90	3.64	γ + γ'									2.07	90		
			2.00 - 2.09													2.07	90	3.58	γ
			1.80 - 1.99	1.81	80	3.62	γ + γ'									1.78			
			1.70 - 1.79													1.78	80	3.56	γ
			1.60 - 1.69													1.60	50		Al_2O_3
			1.50 - 1.59																
			1.40 - 1.49													1.40	30		Al_2O_3
			1.30 - 1.39													1.37	30		Al_2O_3
			1.20 - 1.29													1.26	90	3.56	γ
																1.24	30		Al_2O_3
			1.10 - 1.19													1.19	30		Al_2O_3

TABLE VII (CONT'D)

ELEVATED TEMPERATURE X-RAY DIFFRACTION PATTERNS

(Standard Patterns of γ, γ', α Al_2O_3, Cr_2O_3, and NiO)

d Range	γ		γ'		α Al_2O_3		Cr_2O_3		NiO	
	d	I	d	I	d	I	d	I	d	I
3.90 - > 4.0										
3.80 - 3.89										
3.70 - 3.79										
3.60 - 3.69							3.62	60		
3.50 - 3.59			3.56	70						
3.40 - 3.49					3.48	74				
3.30 - 3.39										
3.20 - 3.29										
3.10 - 3.19										
3.00 - 3.09										
2.70 - 2.99										
2.60 - 2.69							2.66	60		
2.50 - 2.59			2.52	70	2.55	92				
2.40 - 2.49							2.48	80	2.41	70
2.30 - 2.39					2.38	42				
2.20 - 2.29										
2.10 - 2.19					2.17	< 1	2.16	80		
2.00 - 2.09	2.05	90	2.05	90	2.08	100	2.03	40	2.09	100
1.80 - 1.99							1.81	70		
1.70 - 1.79	1.78	90	1.78	90	1.74	43				
1.60 - 1.69			1.60	30	1.60	81	1.67	100		
							1.61	50		
1.50 - 1.59					1.55	3	1.57	-		
					1.51	7				
1.40 - 1.49			1.46	30	1.40	32	1.46	80	1.48	80
							1.43	90		
1.30 - 1.39					1.37	48				
1.20 - 1.29	1.26	90	1.26	90	1.28	2	1.29	70	1.26	60
					1.24	16	1.28	50	1.20	50
							1.24	70		
							1.21	-		
1.10 - 1.19					1.19	6	1.19	-		
							1.17	-		

(1) No suffix refers to the pattern obtained at temperature. The suffixes Q, A, and D refer to the quenched, aged, and Debye patterns respectively.

(2) The temperatures at which the exposures were taken are adjacent to the film numbers.

(4) The suffix sp refers to a spotty diffraction line. No suffix means the line was continuous. The reported intensities are based on the scale: 10-100.

(5) Lattice parameter of lines close to the superlattice reflections were calculated assuming that the questionable lines were the (100) and (110) reflections from the superlattice.

(6) The standard patterns of the γ, γ', and oxides identified in this research are included at the end of the table.

TABLE VIII

COMPARISON OF INTEGRATED INTENSITIES AND INTENSITY RATIOS OF ELEVATED TEMPERATURE DIFFRACTION DIAGRAMS WITH THEORETICAL INTENSITY RATIOS

Heat No.	Temp. °C	Film No.	Experimental Intensities			Theoretical Intensity Ratios	
			$I_{(100)}$	$I_{(111)}$	$I_{(100)}/I_{(111)}$	$I_{(100)}/I_{(111)}$ Assuming Only γ' is Ordered	$I_{(100)}/I_{(111)}$ Assuming Both γ and γ' are Ordered
R 332	893	319	0	8.20	0	0	-
R 333	893	289,290	0	14.70	0	0	0.031
R 334	893	300	0.41	15.12	0.027	0.03	0.037
R 334	982	308	0	15.28	0	0	0.036
R 334	1038	310	0	11.0	0	0	0.036
R 334	1038	321	0	11.38	0	0	0.036
R 334	893	312	0.38	11.94	0.032	0.03	0.037
R 334	893	323	0.19	10.30	0.020	0.03	0.037
R 449	900	267	0.46	8.10	0.057	0.058	0.0585
R 449	1000	271	0.45	10.05	0.045	0.049	0.0535
R 449	1073	284	0.42	13.00	0.032	0.030	0.058
R 449	1073	328	0.79	22.6	0.035	0.030	0.058

TABLE IX

X-RAY DIFFRACTION DIAGRAMS OF SOLID SPECIMENS QUENCHED FROM
THE SINGLE AND TWO-PHASE FIELDS OF THE PHASE DIAGRAM

Heat & Spec. No.	Film No.	Temp. °C	Microstructure as Quenched	d Range	Diffraction Pattern (750°C)				Diffraction Pattern (850°C)				Diffraction Pattern (1000°C)			
					d	$I^{(1)}$	a_o	Ident.(2)	d	$I^{(1)}$	a_o	Ident.(2)	d	$I^{(1)}$	a_o	Ident.(2)
R 332 - 158w	236	750	$\gamma + \gamma'$ at Temp.	3.90 - > 4.0					4.06	20		-				
- 157w	232	850	γ	3.80 - 3.89					3.87	20		-				
- 91w	164	1000	γ	3.70 - 3.79												
				3.60 - 3.69												
				3.50 - 3.59	3.56	30	3.56	γ'								
				3.40 - 3.49												
				3.30 - 3.39												
				3.20 - 3.29	3.26	20		-	3.29	20		-				
				3.10 - 3.19					3.16	20		-				
				3.00 - 3.09									3.09	30		-
				2.70 - 2.99					2.72	20		Cr_2O_3				
				2.60 - 2.69									2.68	20		Cr_2O_3
				2.50 - 2.59	2.54	30	3.59	γ'								
				2.40 - 2.49	2.44	30		Cr_2O_3	2.45	30		Cr_2O_3	2.46	70		Cr_2O_3
				2.30 - 2.39												
				2.20 - 2.29												
				2.10 - 2.19					2.11	20		NiO				
				2.00 - 2.09	2.07	100	3.59	$\gamma + \gamma'$	2.07	100	3.59	γ	2.07	90	3.59	γ
				1.80 - 1.99												
				1.70 - 1.79	1.795	100	3.59	$\gamma + \gamma'$	1.79	100	3.58	γ	1.77	80	3.54	γ
				1.60 - 1.69												
				1.50 - 1.59	1.50	20		-								
				1.40 - 1.49												
				1.30 - 1.39												
				1.20 - 1.29	1.26	100	3.56	$\gamma + \gamma'$	1.265	100	3.58	γ	1.265	90	3.58	γ

TABLE IX (CONT'D)

X-RAY DIFFRACTION DIAGRAMS OF SOLID SPECIMENS QUENCHED FROM
THE SINGLE AND TWO-PHASE FIELDS OF THE PHASE DIAGRAM

Heat & Spec. No.	Film No.	Temp. °C	Microstructure as Quenched	d Range	Diffraction Pattern (750°C)				Diffraction Pattern (850°C)				Diffraction Pattern (950°C)			
					d	I(1)	a_o	Ident.(2)	d	I(1)	a_o	Ident.(2)	d	I(1)	a_o	Ident.(2)
R 333 - 160w	237	750	$\gamma + \gamma$ at Temp.	3.90 - > 4.0												
- 93w	159	850	$\gamma + \gamma$ at Temp.	3.80 - 3.89												
- 159w	234	950	γ	3.70 - 3.79												
				3.60 - 3.69	3.60	70	3.60	γ'								
				3.50 - 3.59					3.57	30	3.57	γ'				
				3.40 - 3.49												
				3.30 - 3.39												
				3.20 - 3.29												
				3.10 - 3.19									3.16	20		-
				3.00 - 3.09					3.06	20		-				
				2.70 - 2.99									2.71	20		Cr_2O_3
				2.60 - 2.69												
				2.50 - 2.59	2.54	70	3.59	γ'	2.53	30	3.58	γ'	2.54	10		Al_2O_3
				2.40 - 2.49	2.46	70		Cr_2O_3	2.44	30		Cr_2O_3				
				2.30 - 2.39												
				2.20 - 2.29												
				2.10 - 2.19					2.13	30		Cr_2O_3				
				2.00 - 2.09	2.07	90	3.59	$\gamma + \gamma'$	2.07	90	3.59	$\gamma + \gamma'$	2.07	100	3.58	γ
				1.80 - 1.99												
				1.70 - 1.79					1.795	80	3.59	$\gamma + \gamma'$	1.79	100	3.58	γ
				1.60 - 1.69					1.60	10	3.58	γ'				
				1.50 - 1.59					1.52	10		NiO				
				1.40 - 1.49												
				1.30 - 1.39												
				1.20 - 1.29	1.26	100	3.56	$\gamma + \gamma'$	1.265	90	3.58	$\gamma + \gamma'$	1.26	100	3.56	γ

TABLE IX (CONT'D)

X-RAY DIFFRACTION DIAGRAMS OF SOLID SPECIMENS QUENCHED FROM THE SINGLE AND TWO-PHASE FIELDS OF THE PHASE DIAGRAM

Heat & Spec. No.	Film No.	Temp. °C	Microstructure as Quenched	d Range	R 333 Diffraction Pattern (1075°C)				R 334 Diffraction Pattern (850°C)				R 334 Diffraction Pattern (1075°C)			
					d	I(1)	a_o	Ident.(2)	d	I(1)	a_o	Ident.(2)	d	I(1)	a_o	Ident.(2)
R 333 - 94w	217	1075	γ	3.90 - > 4.0												
R 334 - 96w	158	850	$\gamma + \gamma'$ at Temp.	3.80 - 3.89												
R 334 - 97w	162	1075	$\gamma + \gamma'$ precipitated during quenching	3.70 - 3.79												
				3.60 - 3.69					3.60	70	3.60	γ'				
				3.50 - 3.59									3.59	60	3.59	γ'
				3.40 - 3.49												
				3.30 - 3.39												
				3.20 - 3.29												
				3.10 - 3.19									3.16	10		-
				3.00 - 3.09	3.09	10		-	3.08	20		-	3.07	10		-
				2.70 - 2.99					2.91	30						
				2.60 - 2.69												
				2.50 - 2.59					2.54	70	3.59	γ'	2.55	30	3.60	γ'
				2.40 - 2.49	2.44	20		Cr_2O_3	2.46	30		Cr_2O_3	2.44	70		Cr_2O_3
				2.30 - 2.39	2.39	20		NiO								
				2.20 - 2.29												
				2.10 - 2.19	2.13	20		Cr_2O_3								
				2.00 - 2.09	2.07	90	3.59	γ	2.07	90	3.59	$\gamma + \gamma'$	2.07	100	3.59	$\gamma + \gamma'$
				1.80 - 1.99												
				1.70 - 1.79	1.79	80	3.58	γ	1.79	90	3.58	$\gamma + \gamma'$	1.79	80	3.58	$\gamma + \gamma'$
				1.60 - 1.69					1.60	30	3.58	γ'	1.60	10	3.58	γ'
				1.50 - 1.59												
				1.40 - 1.49					1.46	30	3.58	γ'	1.46	10	3.58	γ'
				1.30 - 1.39												
				1.20 - 1.29	1.27	20	3.59	γ	1.27	90	3.59	$\gamma + \gamma'$	1.265	100	3.58	$\gamma + \gamma'$

TABLE IX (CONT'D)

X-RAY DIFFRACTION DIAGRAMS OF SOLID SPECIMENS QUENCHED FROM
THE SINGLE AND TWO-PHASE FIELDS OF THE PHASE DIAGRAM

Heat & Spec. No.	Film No.	Temp. °C	Microstructure as Quenched	d Range	Diffraction Pattern (750°C)				Diffraction Pattern (1000°C)				Diffraction Pattern (1150°C)			
					d	$I^{(1)}$	a_o	Ident.(2)	d	$I^{(1)}$	a_o	Ident.(2)	d	$I^{(1)}$	a_o	Ident.(2)
R 379 - 171w	241	750	$\gamma+\gamma'$ at Temp.	3.90 - > 4.0												
- 108w	174	1000	$\gamma+\gamma'$ at Temp.	3.80 - 3.89												
- 147w	211	1150	$\gamma+\gamma'$ precipitated during quenching	3.70 - 3.79												
				3.60 - 3.69					3.60	70	3.60	γ'	3.61	50	3.61	γ'
				3.50 - 3.59	3.59	90	3.59	γ'								
				3.40 - 3.49												
				3.30 - 3.39												
				3.20 - 3.29												
				3.10 - 3.19												
				3.00 - 3.09									3.00	30		-
				2.70 - 2.99	2.70	30		Cr_2O_3								
				2.60 - 2.69												
				2.50 - 2.59	2.54	80	3.59	γ'	2.54	70	3.59	γ'	2.54	50	3.59	γ'
				2.40 - 2.49	2.45	80		Cr_2O_3					2.46	70		Cr_2O_3
				2.30 - 2.39												
				2.20 - 2.29												
				2.10 - 2.19									2.13	50		Cr_2O_3
				2.00 - 2.09	2.07	100	3.59	$\gamma+\gamma'$	2.07	100	3.59	$\gamma+\gamma'$	2.07	90	3.59	$\gamma+\gamma'$
				1.80 - 1.99									1.80	90	3.59	$\gamma+\gamma'$
				1.70 - 1.79	1.795	100	3.59	$\gamma+\gamma'$	1.795	90	3.59	$\gamma+\gamma'$				
				1.60 - 1.69	1.60	60	3.58	γ'	1.60	30	3.58	γ'	1.60	30	3.58	γ'
				1.50 - 1.59					1.50	10		Ni0	1.50	30		Ni0
				1.40 - 1.49	1.46	60	3.58	γ'	1.46	30		γ'	1.46	30	3.58	γ'
				1.30 - 1.39												
				1.20 - 1.29	1.265	100	3.58	$\gamma+\gamma'$	1.26	90	3.56	$\gamma+\gamma'$	1.26	90	3.56	$\gamma+\gamma'$

TABLE IX (CONT'D)

X-RAY DIFFRACTION DIAGRAMS OF SOLID SPECIMENS QUENCHED FROM
THE SINGLE AND TWO-PHASE FIELDS OF THE PHASE DIAGRAM

Heat & Spec. No.	Film No.	Temp. °C	Microstructure as Quenched	d Range	Diffraction Pattern (998°C)				Diffraction Pattern (1098°C)				Diffraction Pattern (1193°C)			
					d	I(1)	a_o	Ident.(2)	d	I(1)	a_o	Ident.(2)	d	I(1)	a_o	Ident.(2)
R 346 - 85w	146	998	$\gamma + \gamma'$ at Temp.	3.90 - > 4.0												
- 68w	118	1098	$\gamma + \gamma'$ at Temp.	3.80 - 3.89												
- 84w	145	1193	$\gamma + \gamma'$ precipitated during quenching	3.70 - 3.79												
				3.60 - 3.69	3.60	80	3.60	γ'								
				3.50 - 3.59					3.59	70	3.59	γ'	3.58	50	3.58	γ'
				3.40 - 3.49												
				3.30 - 3.39												
				3.20 - 3.29												
				3.10 - 3.19												
				3.00 - 3.09					3.08	10		-				
				2.70 - 2.99												
				2.60 - 2.69									2.69	10		Cr_2O_3
				2.50 - 2.59	2.54	80	3.59	γ'	2.53	70	3.58	γ'	2.54	70	3.59	γ'
				2.40 - 2.49	2.46	30		Cr_2O_3	2.46	30		Cr_2O_3	2.46	20		Cr_2O_3
				2.30 - 2.39												
				2.20 - 2.29												
				2.10 - 2.19	2.12	30		Cr_2O_3								
				2.00 - 2.09	2.07	90	3.59	$\gamma + \gamma'$	2.07	90	3.59	$\gamma + \gamma'$	2.07	100	3.59	$\gamma + \gamma'$
				1.80 - 1.99												
				1.70 - 1.79	1.78	90	3.56	$\gamma + \gamma'$	1.79	90	3.58	$\gamma + \gamma'$	1.79	90	3.58	$\gamma + \gamma'$
					1.76	30		-								
				1.60 - 1.69	1.60	30	3.58	γ'	1.61	30	3.60	γ'	1.605	30	3.59	γ'
				1.50 - 1.59												
				1.40 - 1.49	1.46	30	3.58	γ'	1.47	30	3.60	γ'	1.46	30	3.58	γ'
				1.30 - 1.39												
				1.20 - 1.29	1.26	90	3.56	$\gamma + \gamma'$	1.27	90	3.59	$\gamma + \gamma'$	1.27	90	3.59	$\gamma + \gamma'$

TABLE IX (CONT'D)

X-RAY DIFFRACTION DIAGRAMS OF SOLID SPECIMENS QUENCHED FROM
THE SINGLE AND TWO-PHASE FIELDS OF THE PHASE DIAGRAM

Heat & Spec. No.	Film No.	Temp. °C	Microstructure as Quenched	d Range	Diffraction Pattern (750°C)				Diffraction Pattern (1000°C)				Diffraction Pattern (1098°C)			
					d	$I^{(1)}$	a_o	Ident.(2)	d	$I^{(1)}$	a_o	Ident.(2)	d	$I^{(1)}$	a_o	Ident.(2)
R 347 - 82a	243	750	$\gamma+\gamma'$ at Temp.	3.90 - > 4.0												
- 66a	242	1000	$\gamma+\gamma'$ at Temp.	3.80 - 3.89					3.81	20		-				
- 83w	143	1098	$\gamma+\gamma'$ at Temp.	3.70 - 3.79												
			+ some γ' pre-	3.60 - 3.69	3.60	80	3.60	γ'	3.60	70	3.60	γ'				
			cipitation	3.50 - 3.59									3.59	80	3.59	γ'
			during quench-	3.40 - 3.49												
			ing	3.30 - 3.39					3.31	20		-				
				3.20 - 3.29					3.21	20		-				
				3.10 - 3.19												
				3.00 - 3.09												
				2.70 - 2.99												
				2.60 - 2.69												
				2.50 - 2.59	2.55	80	3.60	γ'	2.55	70	3.60	γ'	2.54	80	3.59	γ'
				2.40 - 2.49					2.46	70		Cr_2O_3	2.47	70		Cr_2O_3
				2.30 - 2.39												
				2.20 - 2.29												
				2.10 - 2.19												
				2.00 - 2.09	2.07	100	3.59	$\gamma+\gamma'$	2.07	100	3.59	$\gamma+\gamma'$	2.07	90	3.59	$\gamma+\gamma'$
				1.80 - 1.99												
				1.70 - 1.79	1.795	100	3.59	$\gamma+\gamma'$	1.795	100	3.59	$\gamma+\gamma'$	1.795	90	3.59	$\gamma+\gamma'$
				1.60 - 1.69	1.605	70	3.59	γ'	1.605	20	3.59	γ'	1.66	20		Cr_2O_3
													1.60	30	3.58	γ'
				1.50 - 1.59	1.50	30		NiO					1.50	20		NiO
				1.40 - 1.49	1.46	70	3.58	γ'	1.46	20	3.58	γ'	1.47	30	3.59	γ'
				1.30 - 1.39												
				1.20 - 1.29	1.26	100	3.56	$\gamma+\gamma'$	1.26	100	3.56	$\gamma+\gamma'$	1.26	90	3.56	$\gamma+\gamma'$
				1.10 - 1.19												

TABLE IX (CONT'D)

X-RAY DIFFRACTION DIAGRAMS OF SOLID SPECIMENS QUENCHED FROM THE SINGLE AND TWO-PHASE FIELDS OF THE PHASE DIAGRAM

Heat No.	Film No.	Temp. °C	Microstructure as Quenched	d Range	Diffraction Pattern (1200°C) d	I(1)	a_o	Ident.(2)
R 347 - 66w	119	1200	$\gamma+\gamma'$ precipitated during quenching	3.90 - > 4.0				
				3.80 - 3.89				
				3.70 - 3.79				
				3.60 - 3.69	3.61	30	3.61	γ'
				3.50 - 3.59				
				3.40 - 3.49				
				3.30 - 3.39				
				3.20 - 3.29				
				3.10 - 3.19				
				3.00 - 3.09	3.09	20		-
				2.70 - 2.99				
				2.60 - 2.69				
				2.50 - 2.59	2.56	20	3.61	γ'
				2.40 - 2.49	2.46	20		Cr_2O_3
				2.30 - 2.39				
				2.20 - 2.29				
				2.10 - 2.19				
				2.00 - 2.09	2.07	90	3.59	$\gamma + \gamma'$
				1.80 - 1.99	1.795	80	3.59	$\gamma + \gamma'$
				1.70 - 1.79				
				1.60 - 1.69	1.61	20	3.60	γ'
				1.50 - 1.59				
				1.40 - 1.49				
				1.30 - 1.39				
				1.20 - 1.29	1.27	80	3.59	$\gamma + \gamma'$

(1) The reported intensities are based on the scale 10 - 100.

(2) The standard patterns for γ, γ', Cr_2O_3, Al_2O_3, and NiO are included in Table VII.

TABLE X

PARTICLE SIZES OF γ' PRECIPITATED DURING QUENCHING OF SOLID SPECIMENS OF R 380 INTO ICE-BRINE, WATER, OIL AND AIR BATHS

Sample No.	Quenching Bath	Vol. % γ'	Measured Particle Size Å
R 380 - 225	ice-brine	53.4	730
- 226	water	53.4	892
- 227	oil	53.8	1110
- 228	air	57.4	1520

TABLE XI

ELEVATED TEMPERATURE PROPERTIES OF TYPICAL Ni-Cr-Al ALLOYS

Hot Tensile Tests

Spec. No.	Temp.(°F)	T.S.	Y.S.	% Elong.
R 447 - 2	1382	33,400	14,000	82
R 447 - 3	1382	31,800	14,200	90
R 448 - 3	1382	81,800	81,800	2
R 448 - 1	1382	79,400	79,400	1-2
R 448 - 6	1382	76,900	76,900	1-2

Creep Tests

Spec. No.	Temp.	Stress	Min. Creep Rate (%/hr)	% Elong.	Rupture Time
R 447 - 4	1382	4,000	0.00069	-	test stopped before rupture
R 447 - 5	1382	6,000	0.0124	-	test stopped before rupture
R 447 - 6	1382	8,000	0.073	5.7	test stopped before rupture
R 447 - 1	1382	10,000	0.258	7.3	162
R 448 - 3	1382	30,000	0.0036	1	36.1
R 448 - 5	1382	30,000	0.0032	1.6	76.8
R 448 - 7	1382	25,000	0.00092	-	89.4
R 448 - 2	1382	25,000	0.0011	1.9	141.6
R 448 - 8	1382	20,000	0.000361	-	test stopped before rupture

TABLE XII

PROPERTIES OF CAST Ni-Cr-Al ALLOYS

		Tensile Data			Creep Data		
Spec. No.	Temp.	T.S.	Y.S.	% Elong.	Stress	Creep Rate %/hr.	Rupture Time (hr.)
R 437 - 6	1382	27,900	17,800	16			
- 8	1382				8,000	0.119	49.1
- 3	1382				15,000	2.60	86 (min.)
- 7	R.T.	70,800	22,000	53			
R 436 - 8	1382				8,000	-	18 (min.)
- 1	1382	15,700	15,700	-			
- 6	1382	15,050	15,050	0-1			
- 7	R.T.	79,700	-	10			
R 438 - 5	1382	10,970	10,950	1			
- 4	1382	1,840	1,840	0			

FIGURES 1 THRU 26

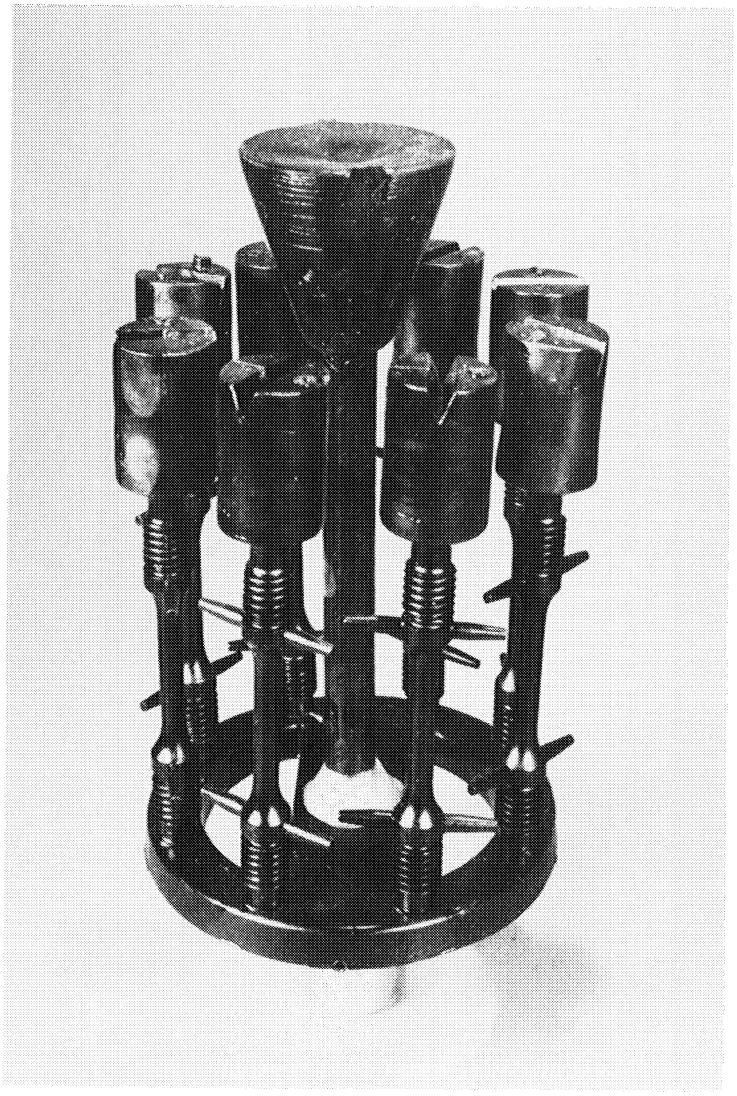

Figure 1. Photograph of a Pattern of Wax Tensile Specimens Illustrating the Gating System Used.

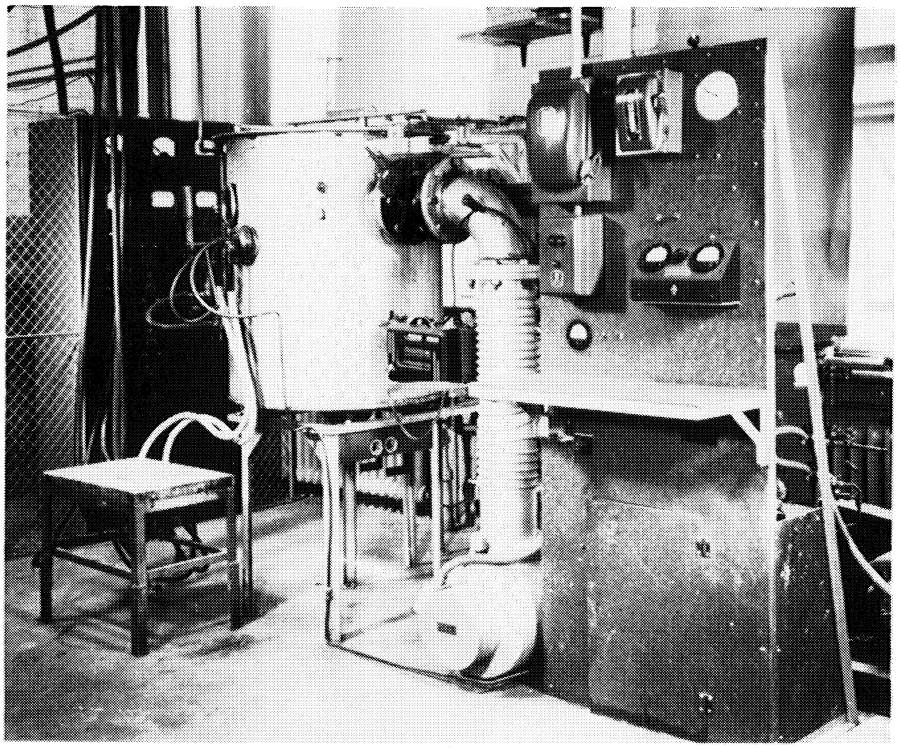

Figure 2. Photograph of Vacuum Induction Melting Equipment Showing Control Panels, Melting Shell, and Vacuum Pumps.

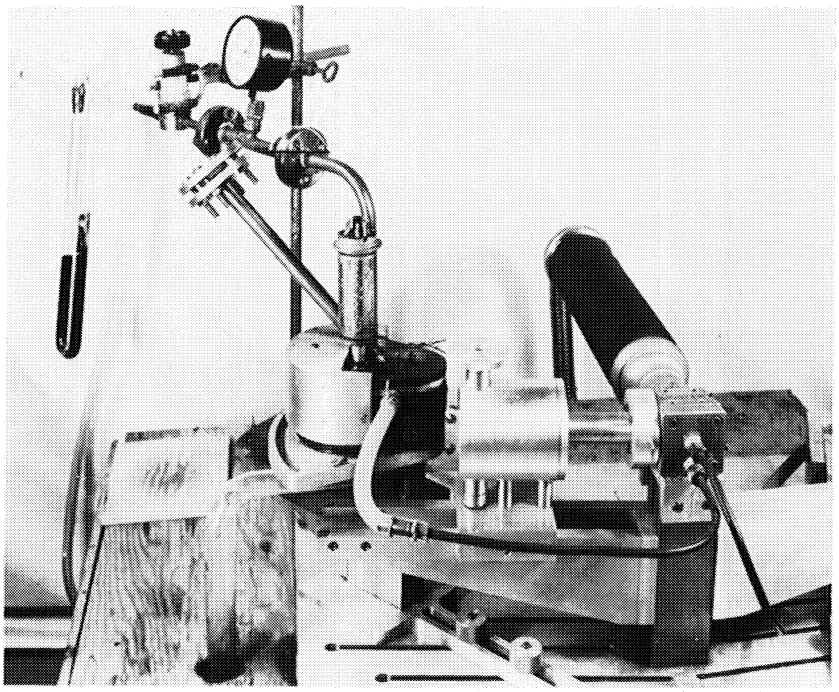

Figure 3. Elevated Temperature X-Ray Diffraction Apparatus Showing X-Ray Tube, Crystal Monochomator, Camera, and Vacuum and Gas Purification Equipment.

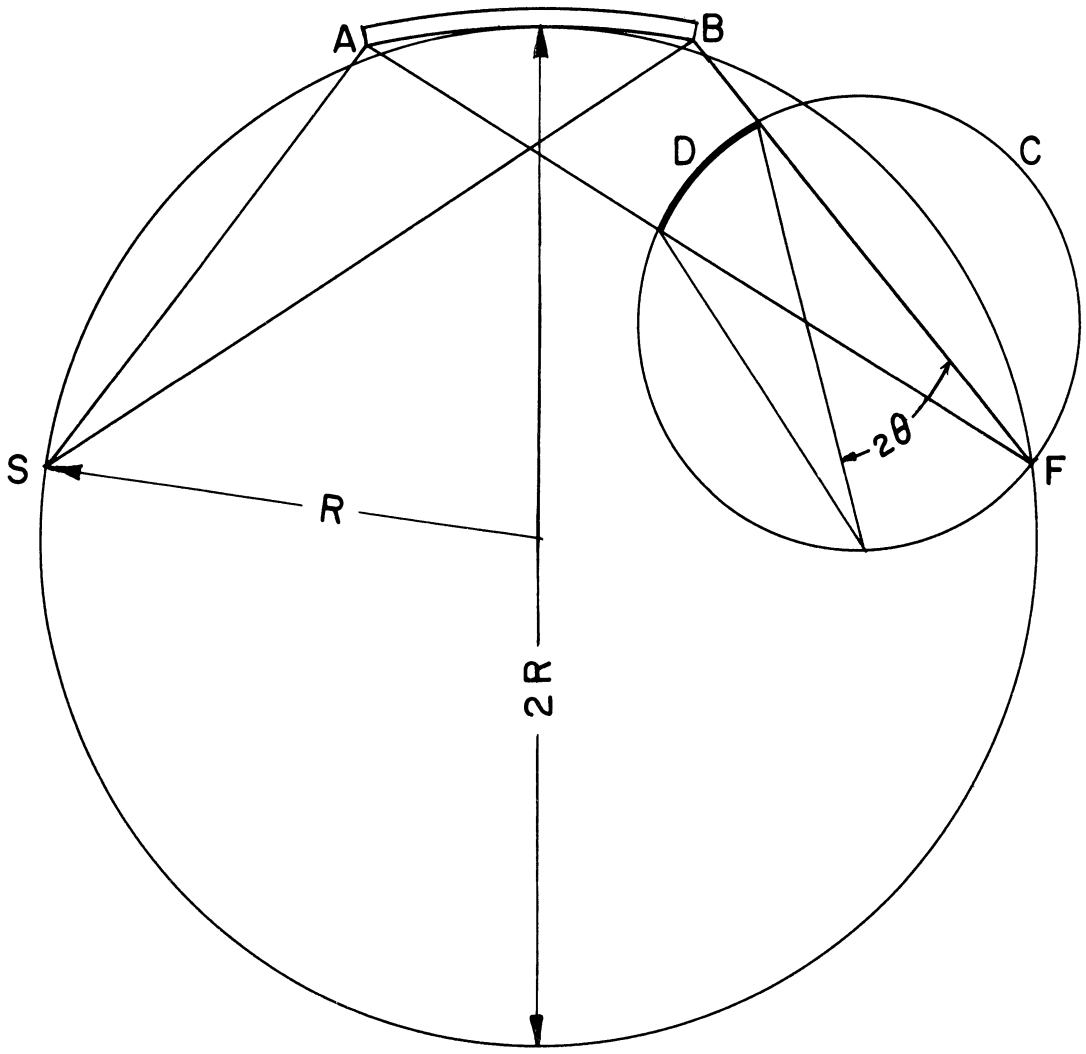

S = SOURCE, X-RAY TUBE
A-B = MONOCHROMATOR
D = FOIL SPECIMEN (NOT BENT)
C = X-RAY CAMERA, DIFFRACTION AREA
F = FOCUS
R = RADIUS OF FOCUSING CIRCLE

Figure 4. Schematic Diagram of X-Ray Geometry Used in Elevated Temperature X-Ray Diffraction.

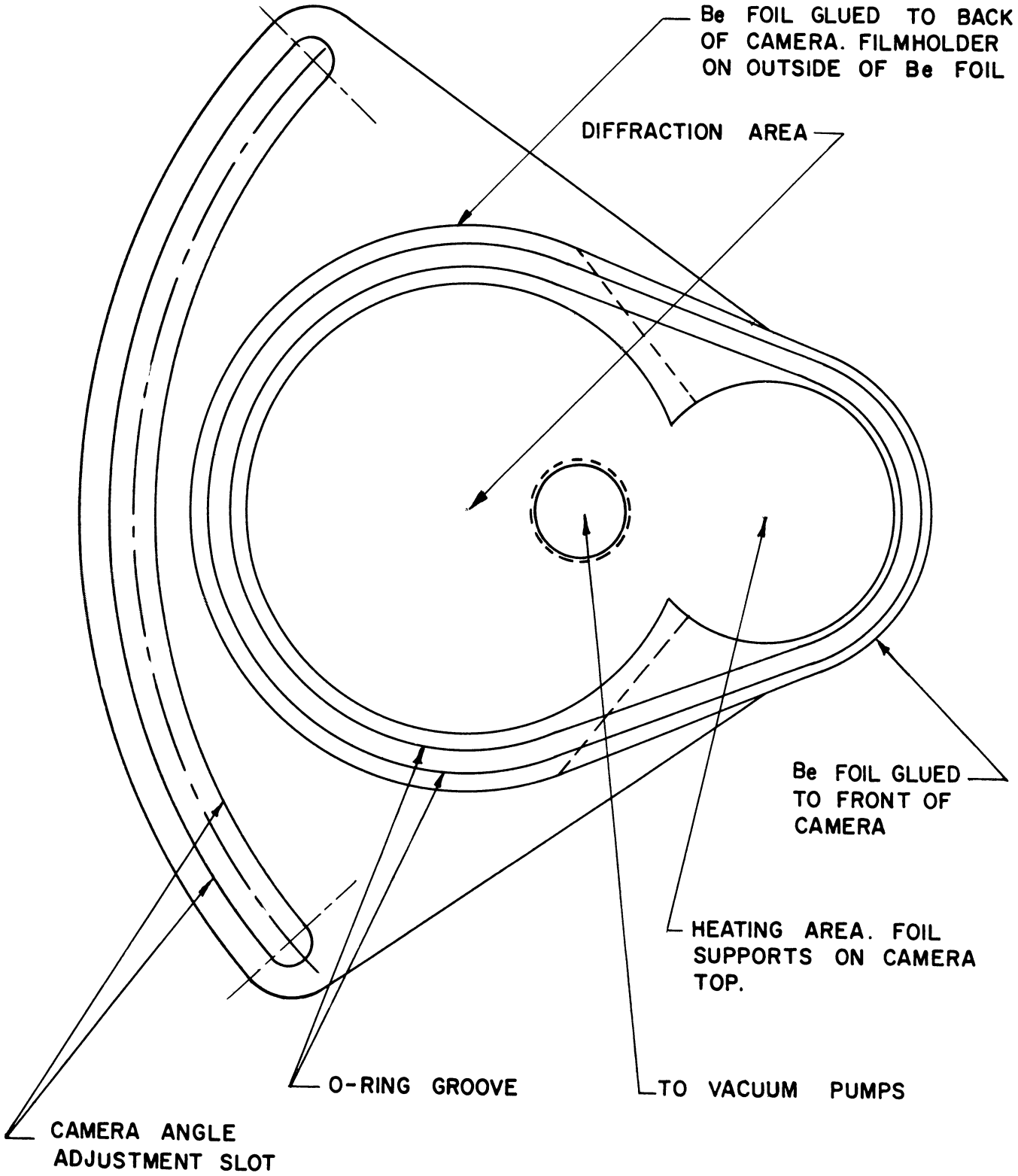

Figure 5. Details of X-Ray Diffraction Camera, Top View
Scale 1:1 Approximately.

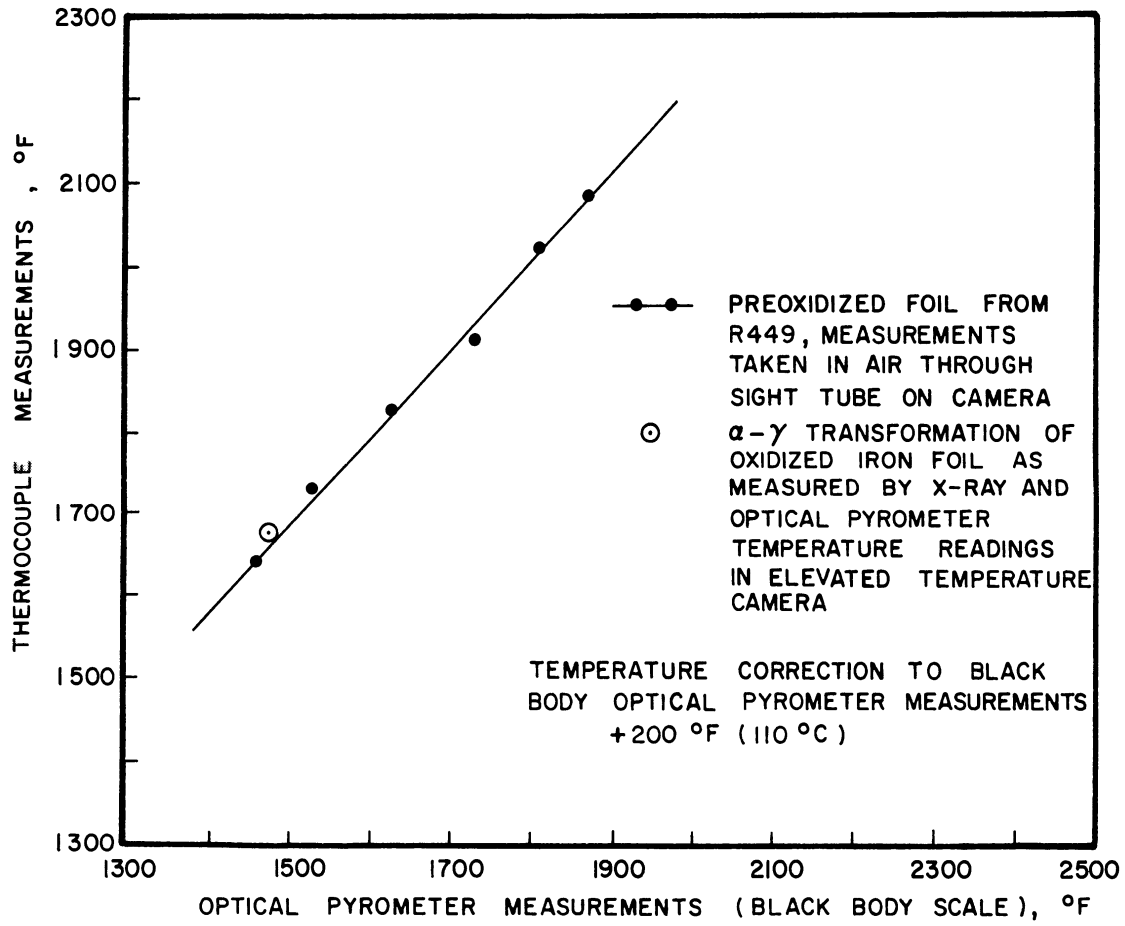

Figure 6. Calibration of Optical Pyrometer Used to Measure Temperatures of Elevated Temperature Diffraction Specimens.

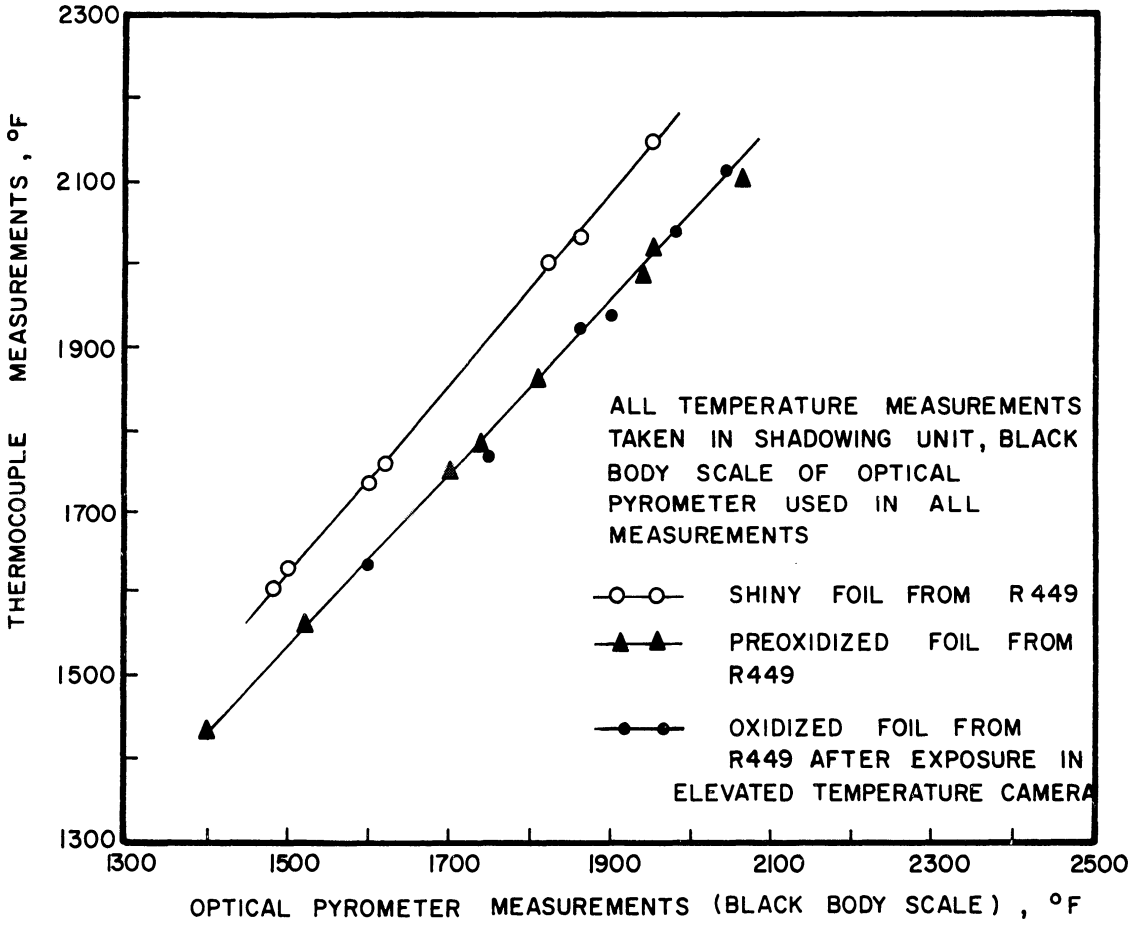

Figure 7. Effect of the Condition of the Foil Surface on Temperature Measurements.

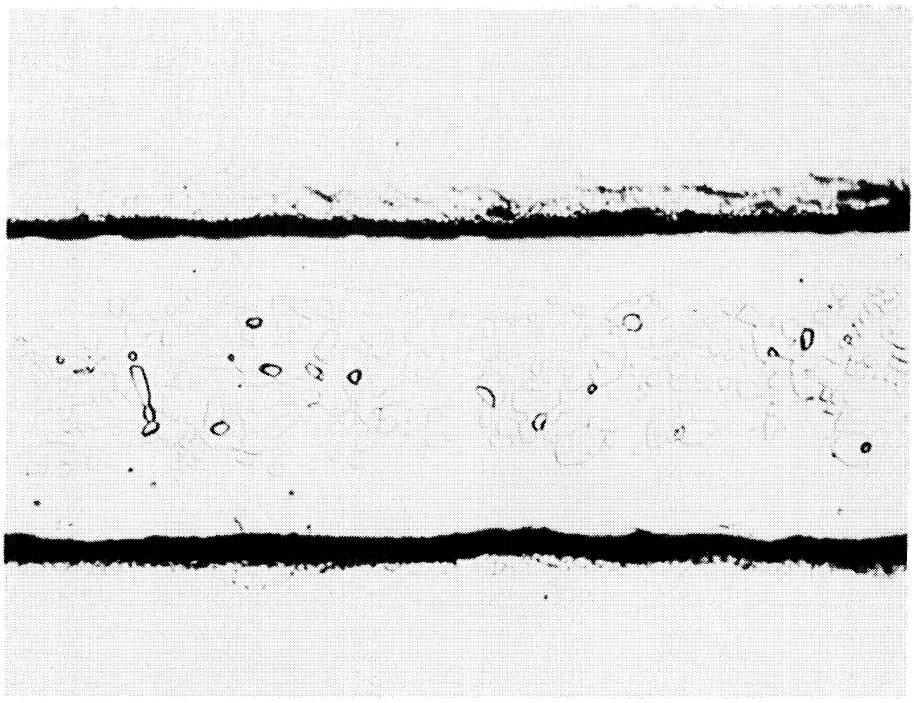

The dark areas between the foil surfaces and Ni plate are crevices from electrolytic etching. The etching solution preferentially attacked the nickel plate rather than the foil specimen. Depletion of γ' from the surface indicated that vaporization of Al and probably Cr had occurred.

Foil: Heat R 449
Temperature: 1073°C (1962°F)
Time at Temperature: 90 hours
Atmosphere: 0.01 micron vacuum
Magnification: 1000X

Figure 8. Vaporization of Aluminum From a Foil Surface.

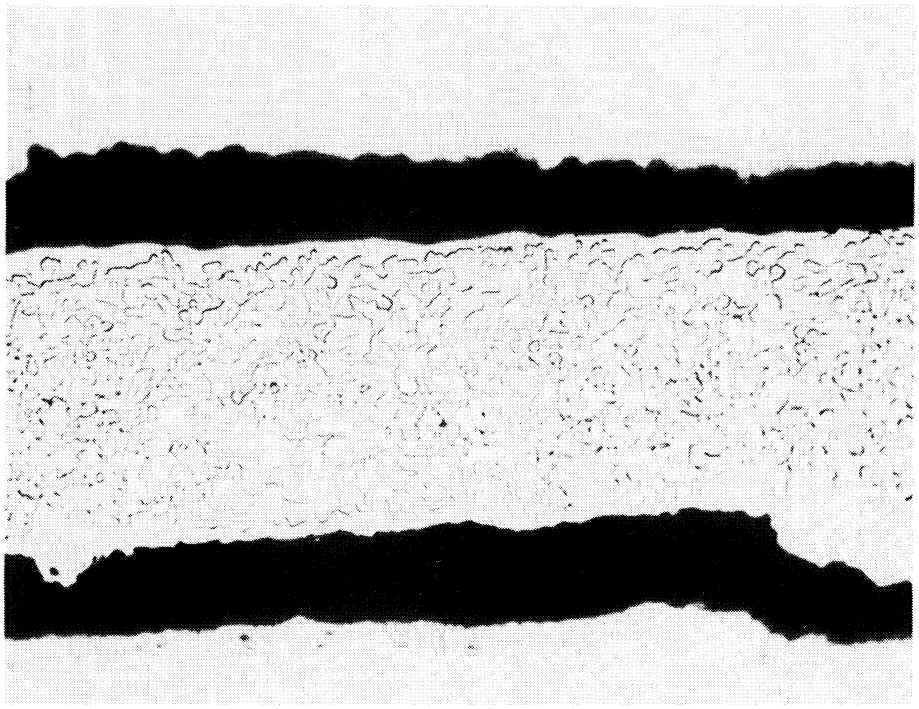

The dark areas between the foil surfaces and Ni plate are crevices from electrolytic etching. The etching solution preferentially attacked the nickel plate rather than the foil specimen. Note little or no surface depletion of γ'.

Foil: Heat R 449
Temperature: 1073°C (1962°F)
Time at Temperature: 90 hours
Atmosphere: 600 millimeters of helium
Magnification: 1000X

Figure 9. Suppression of Aluminum Vaporization with Helium.

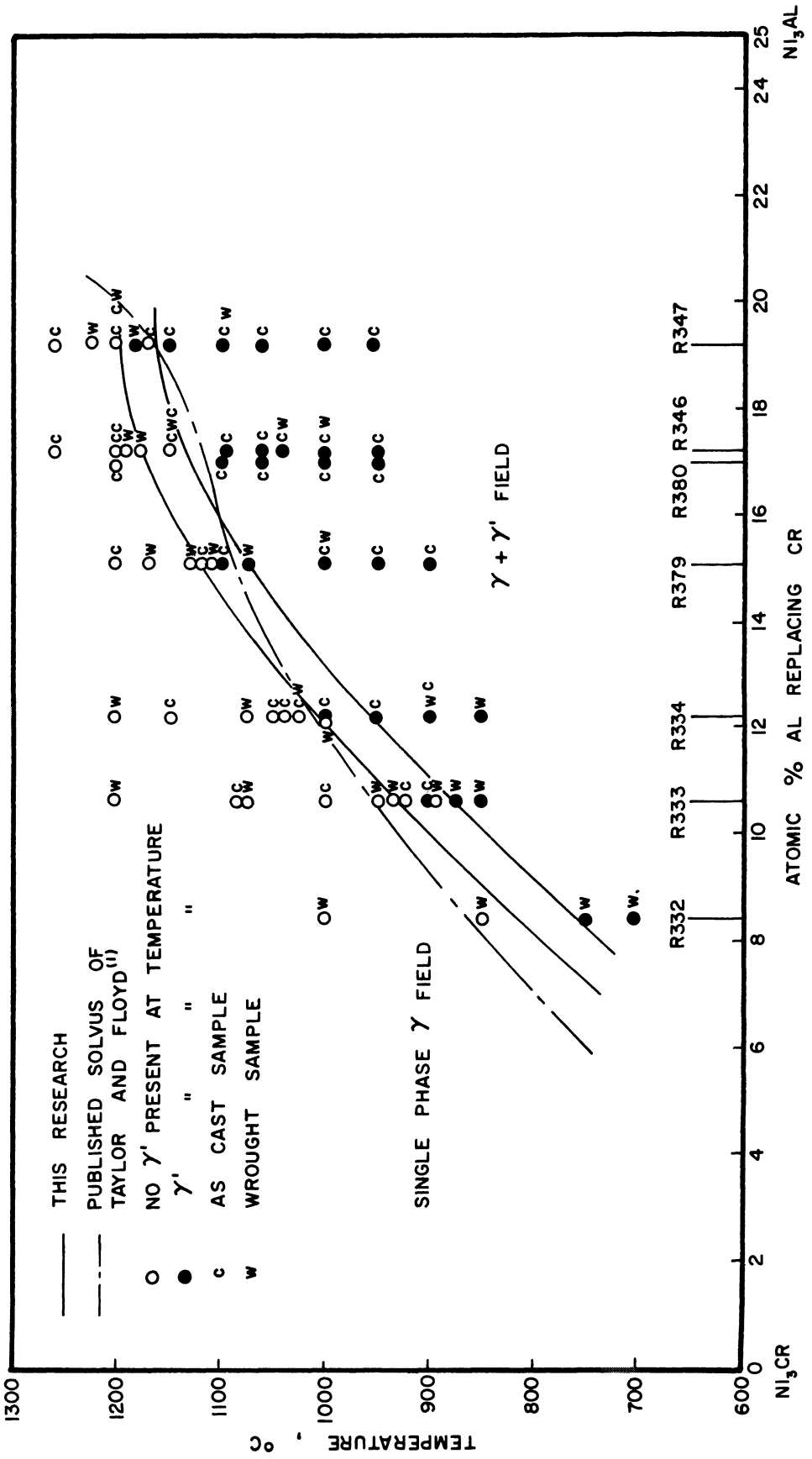

Figure 10. Solvus Band for 12 Hour Solution Treatments for Alloys of Compositions from Ni_3Cr to Ni_3Al.

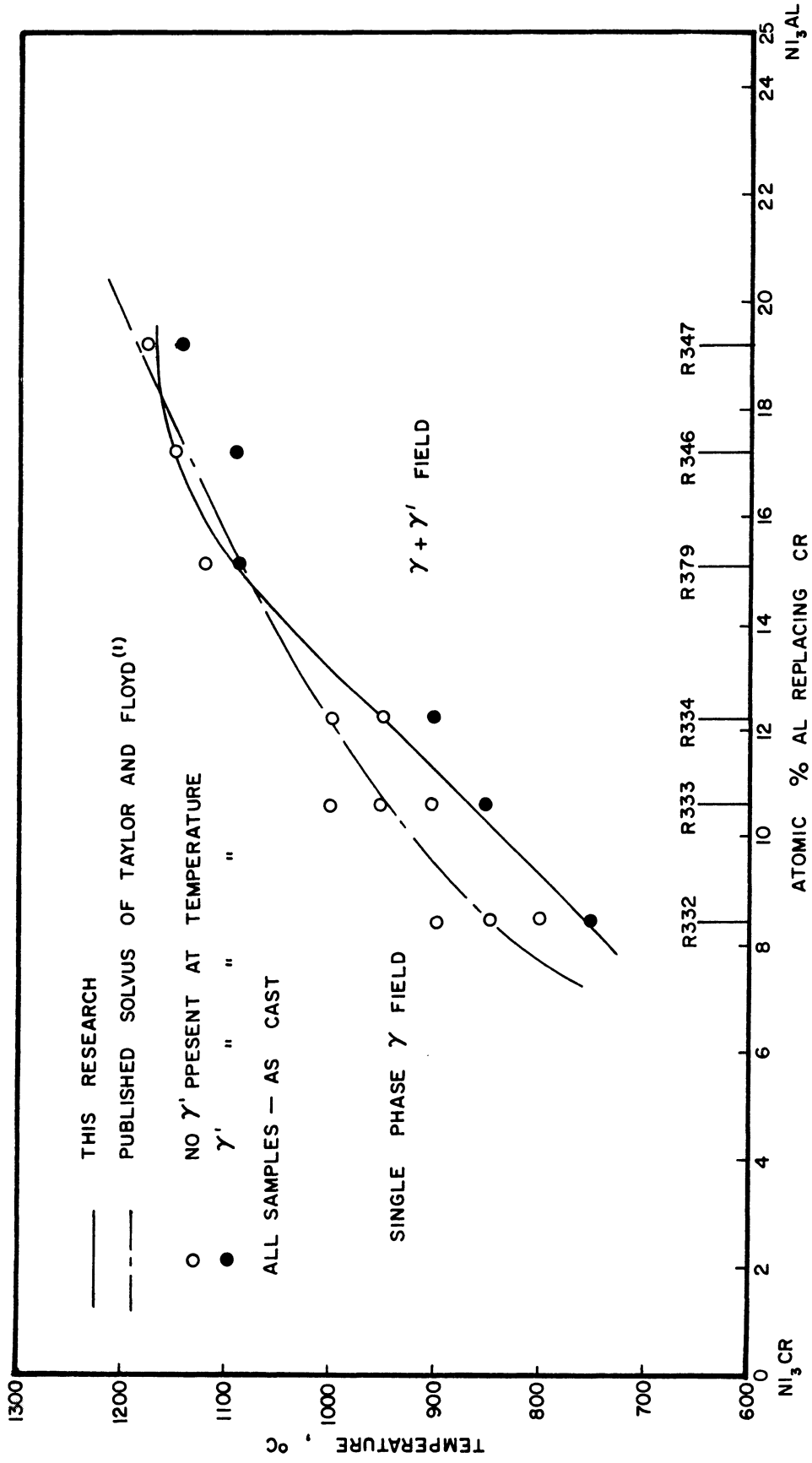

Figure 11. Equilibrium Solvus for Alloys of Compositions from Ni_3Cr to Ni_3Al.

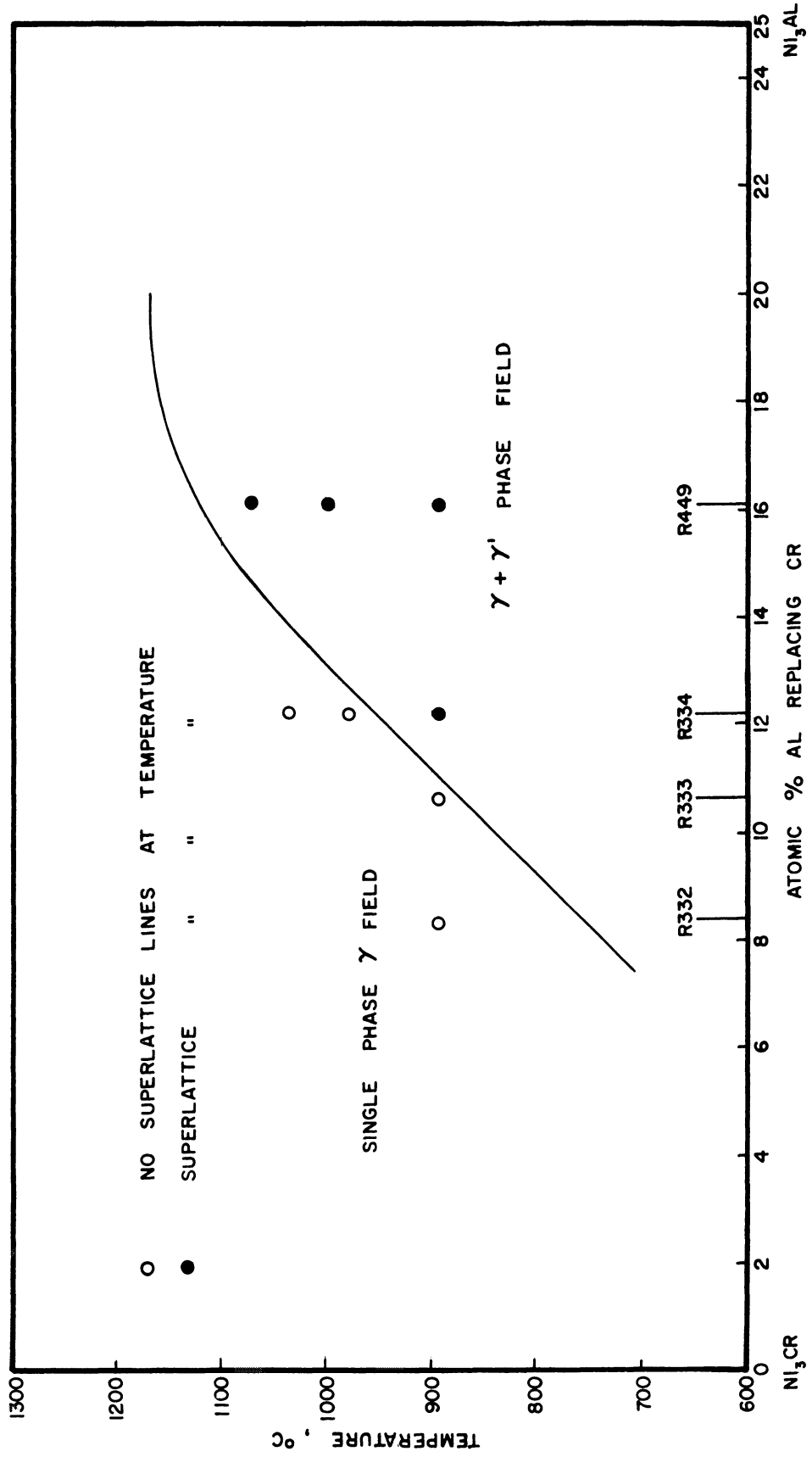

Figure 12. Summary of Elevated Temperature X-Ray Diffraction Results.

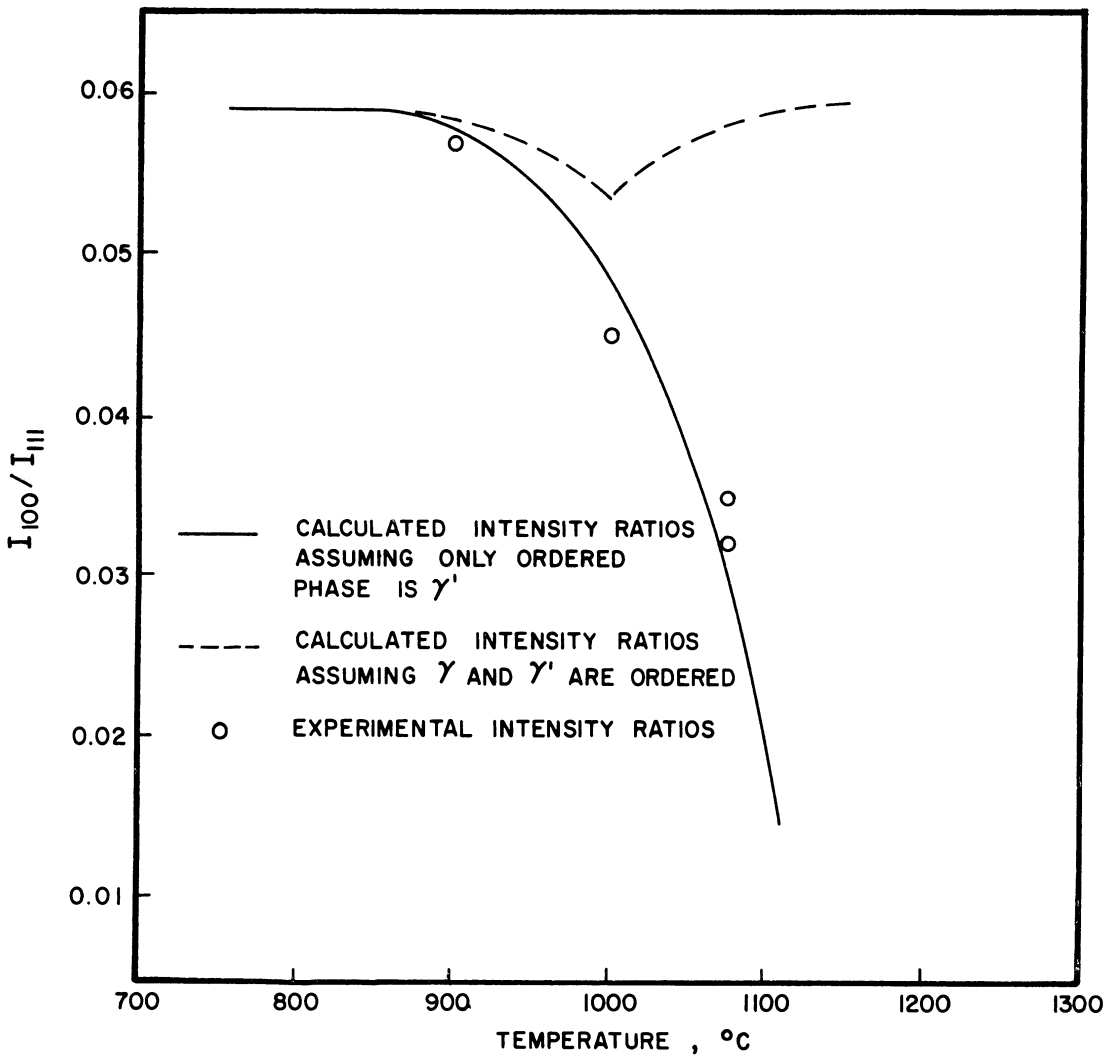

Figure 13. Correlation of Theoretical and Experimental Integrated Intensity Ratios with Temperature for Heat R 449.

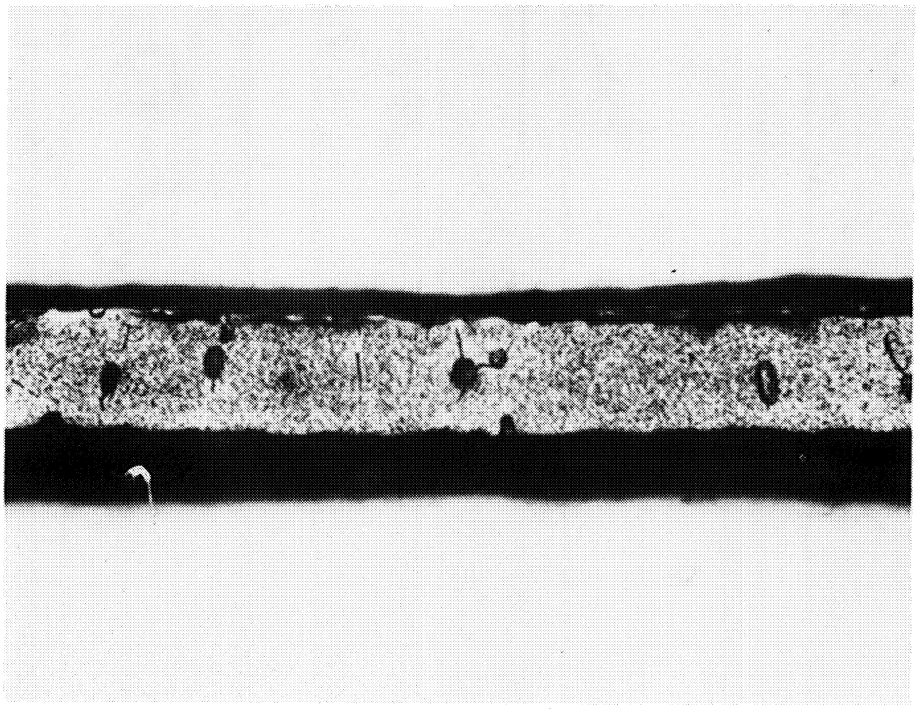

γ' particles are uniform from surface to center denoting no depletion of Al by vaporization or oxidation. The dark areas between the foil surface and the surrounding Ni plate are crevices from electrolytic etching. The etching solution preferentially attacked the nickel plate rather than the foil specimen.

Film No. 300
Magnification: 1000X

Figure 14. Microstructure of Foil R 334 Heated and Exposed at 750°C (1382°F) for 72 Hours.

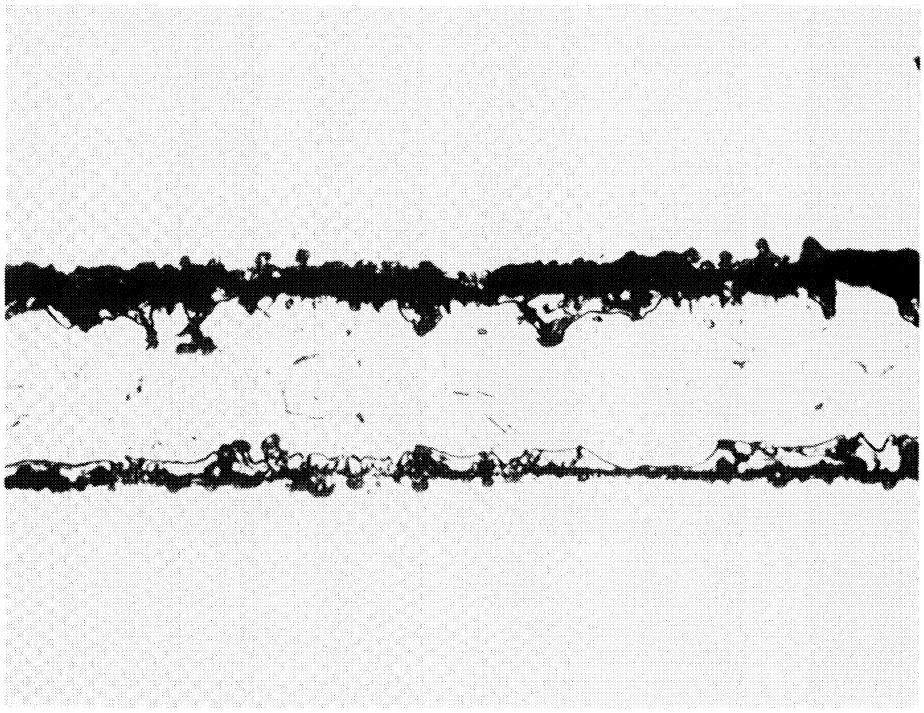

The foil structure, outlined between the dark oxide and crevices between the nickel plate and foil, contains no γ'. The etching solution preferentially attacked the nickel plate rather than the foil specimen. Oxide stringers are present in the foil.

Film No's. 319, 289, and 290
Magnification: 1000X

Figure 15. Typical Foil Microstructure of R 332, 333, or 334 After Exposure in the Single Phase Field for 72 Hours and Quenched in the Helium Atmosphere.

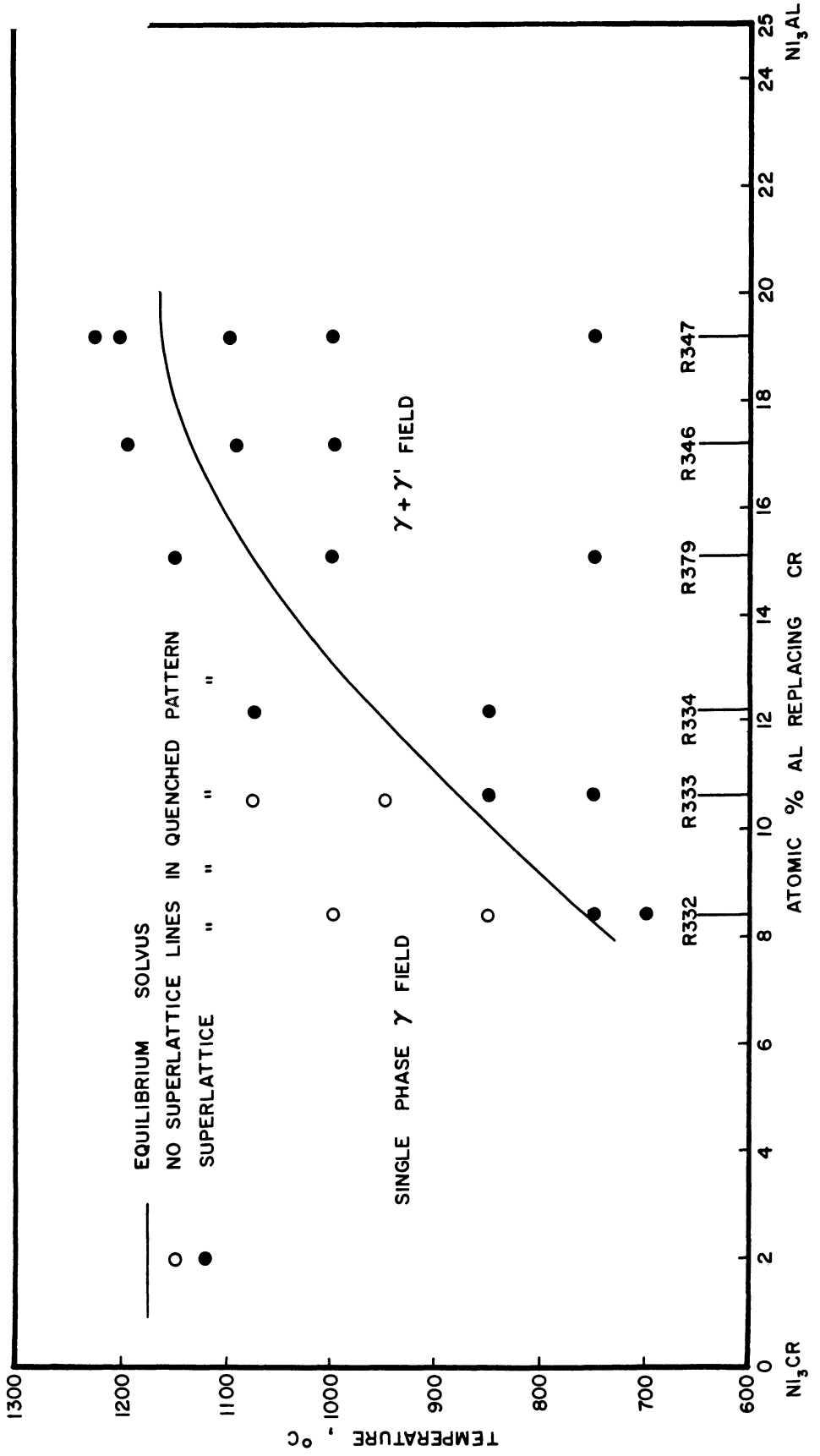

Figure 16. Summary of Ambient Temperature X-Ray Diffraction Results.

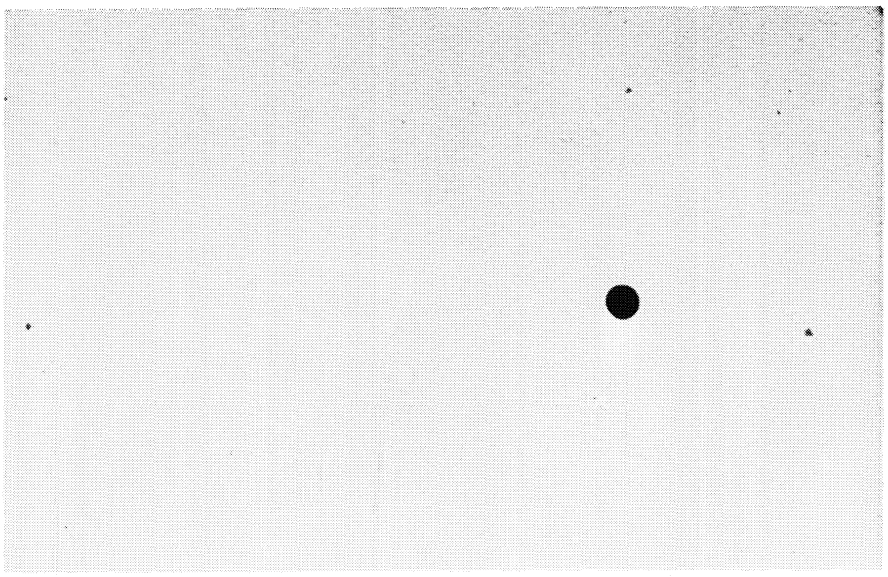

Heat Treatment: 1132°C (2068°F) - 12 hours
Quenching Time: Approximately 1 sec.
Magnification: 12,000X

Figure 17. Pebbly Appearance of Microstructure of Heat R 380 After Quenching in Ice-Brine from the Single Phase γ Field.

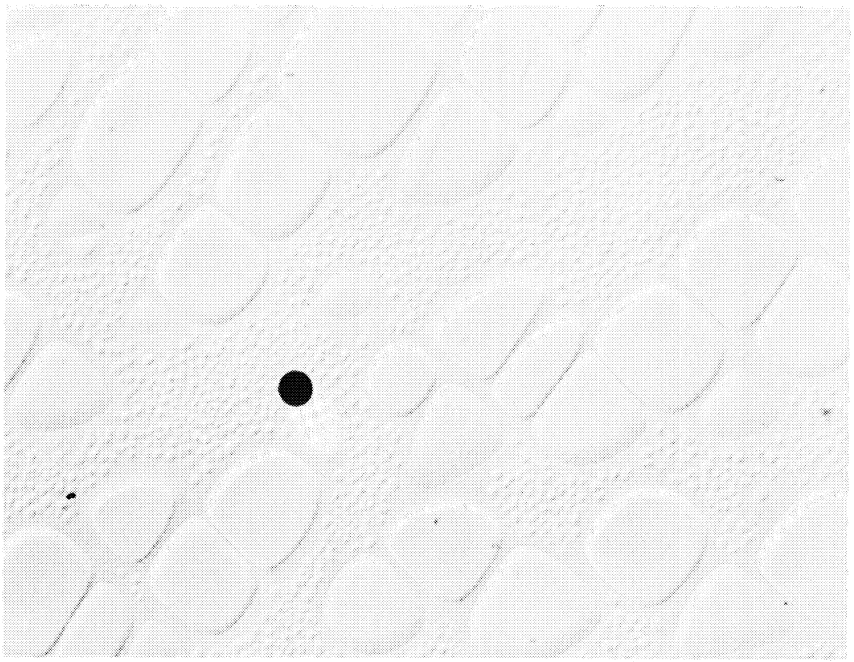

Larger γ' particles present at temperature; smaller particles precipitated during the quenching operation.

Heat Treatment: 1100°C (2012°F) - 12 hours
Quenching Time: Approximately 1 sec.
Magnification: 12,000X

Figure 18. Precipitation of γ' in Heat R 380 During Ice-Brine Quenching from a Temperature Near the Solvus.

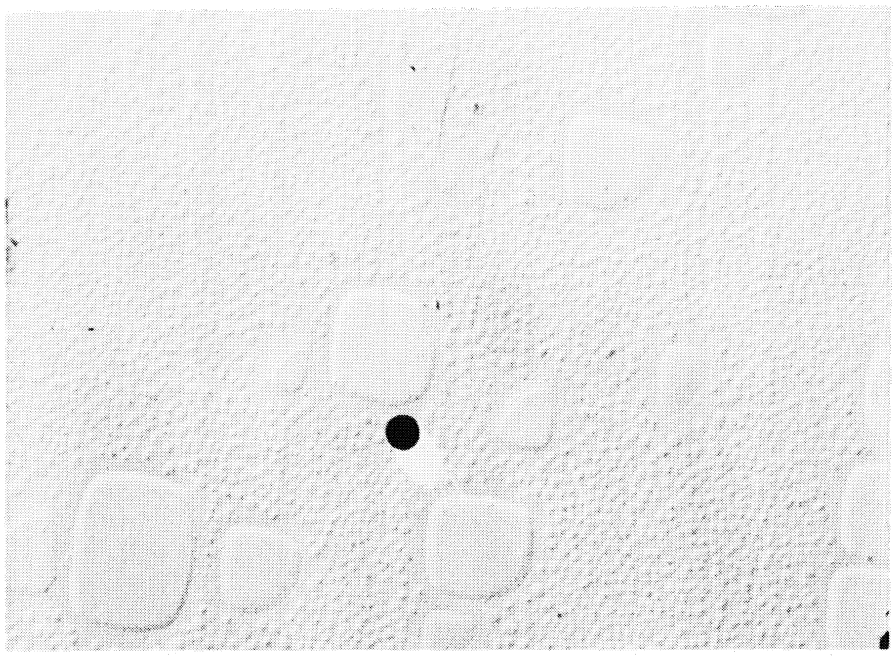

Larger γ' particles present at temperature; smaller particles precipitated during the quenching operation.

Heat Treatment: 1100°C (2012°F) - 12 hours
Quenching Time: Approximately 1 sec.
Magnification: 12,000X

Figure 19. Precipitation of γ' in Heat R 379 During Ice-Brine Quenching from a Temperature Near the Solvus.

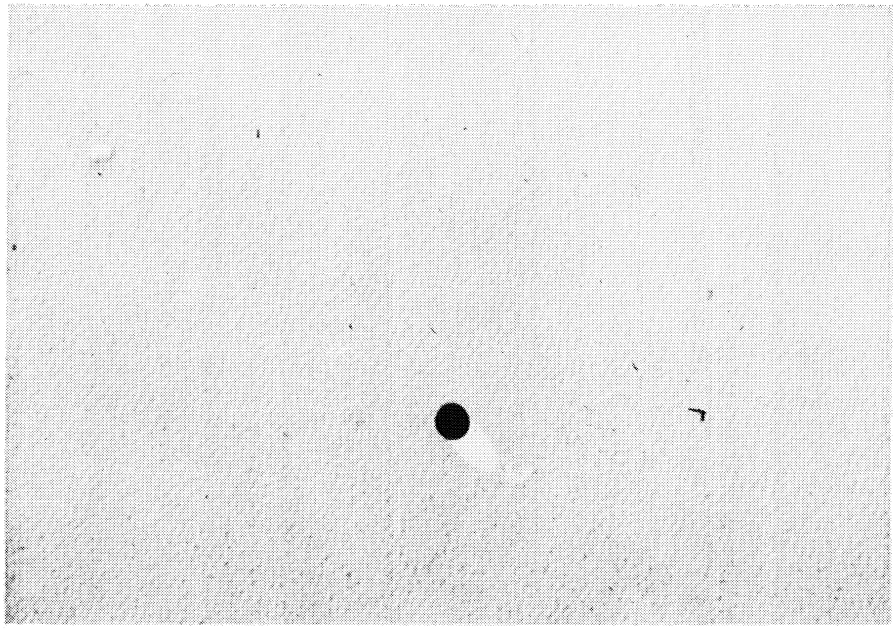

Heat Treatment: 1177°C (2150°F) - 168 hours
Quenching Time: Approximately 1 sec.
Magnification: 12,000X

Figure 20. Pebbly Appearance of Microstructure of Heat R 347 After Quenching from the Single Phase γ Field.

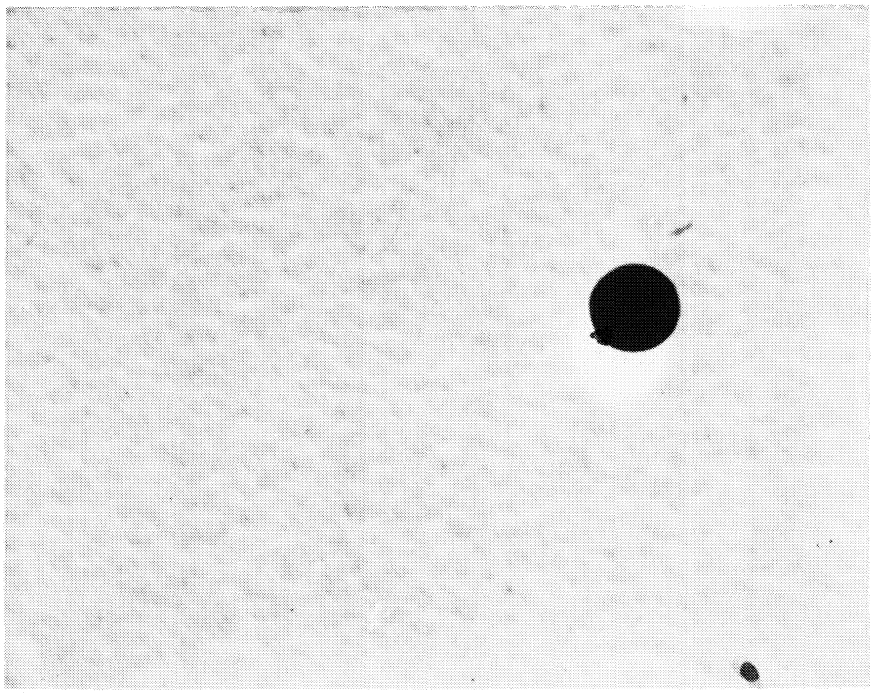

Heat Treatment: 1200°C (2192°F) - 12 hours
Quenching Time: Approximately 1/10 sec.
Particle Size: 892Å
Magnification: 27,600X

Figure 21. Precipitation of γ' in Heat R 380 During Water Quenching from a Vertical Tube Furnace.

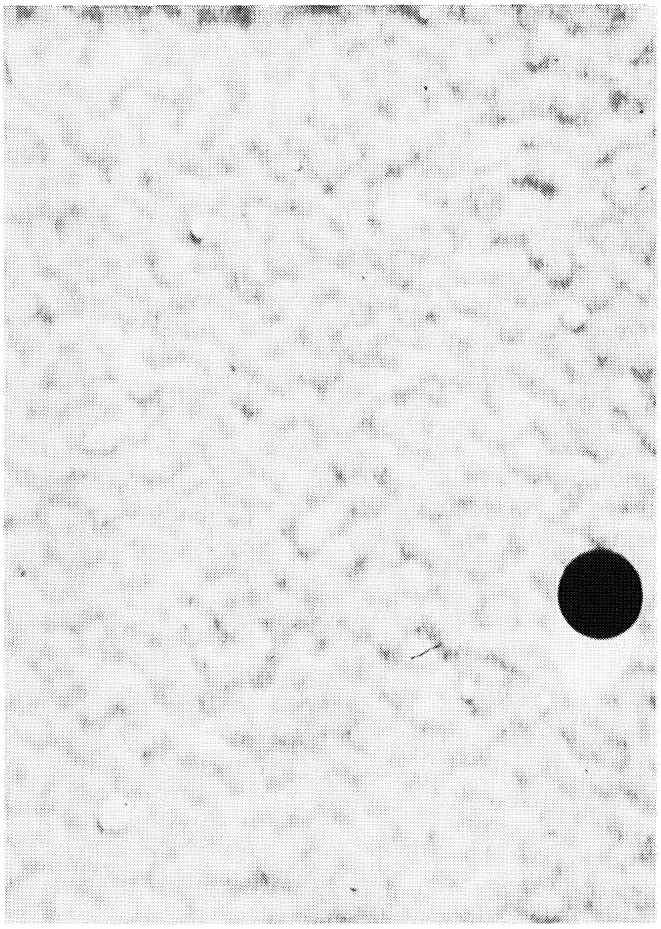

Heat Treatment: 1200°C (2192°F) - 12 hours
Quenching Time: Approximately 1/10 sec.
Particle Size: 1110Å
Magnification: 27,600X

Figure 22. Precipitation of γ' in Heat R 380 During Oil Quenching from a Vertical Tube Furnace.

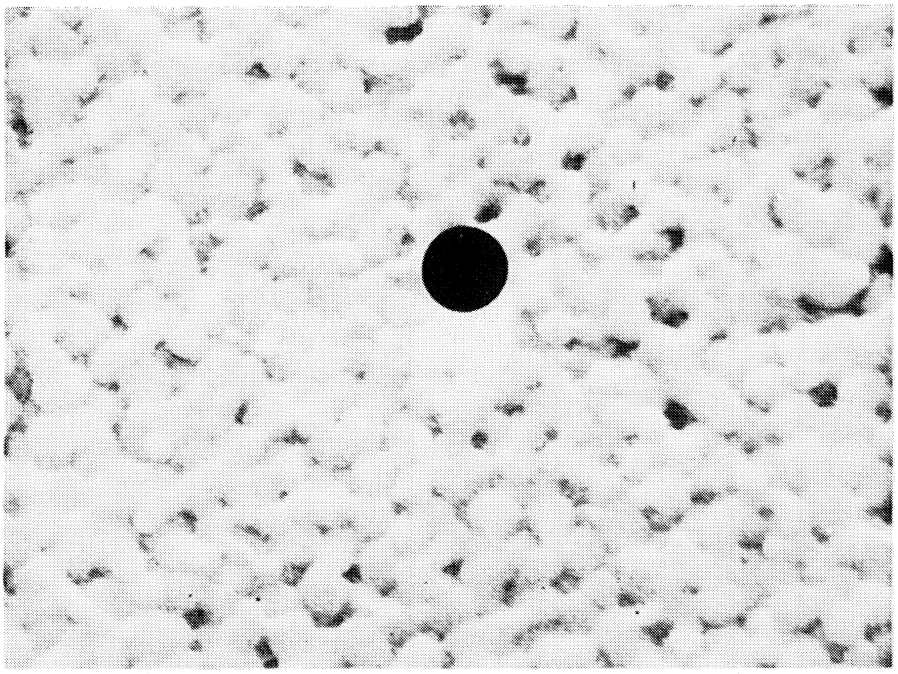

Heat Treatment: 1200°C (2192°F) - 12 hours
Quenching Time: Approximately 1/10 sec.
Particle Size: 1520Å
Magnification: 27,600X

Figure 23. Precipitation of γ' in Heat R 380 During Air Cooling from a Vertical Tube Furnace.

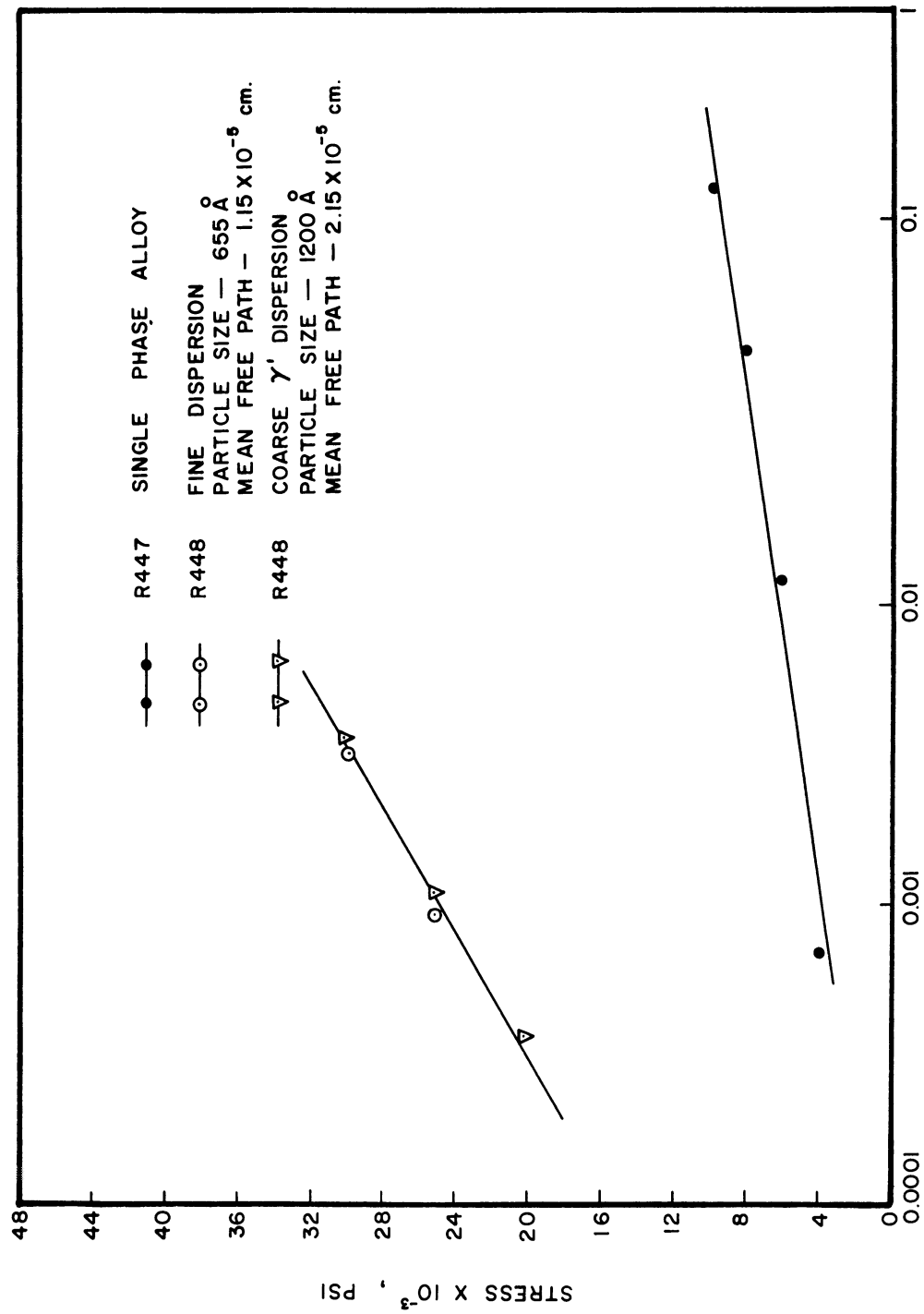

Figure 24. Elevated Temperature Properties of Ni-Cr-Al Alloys.

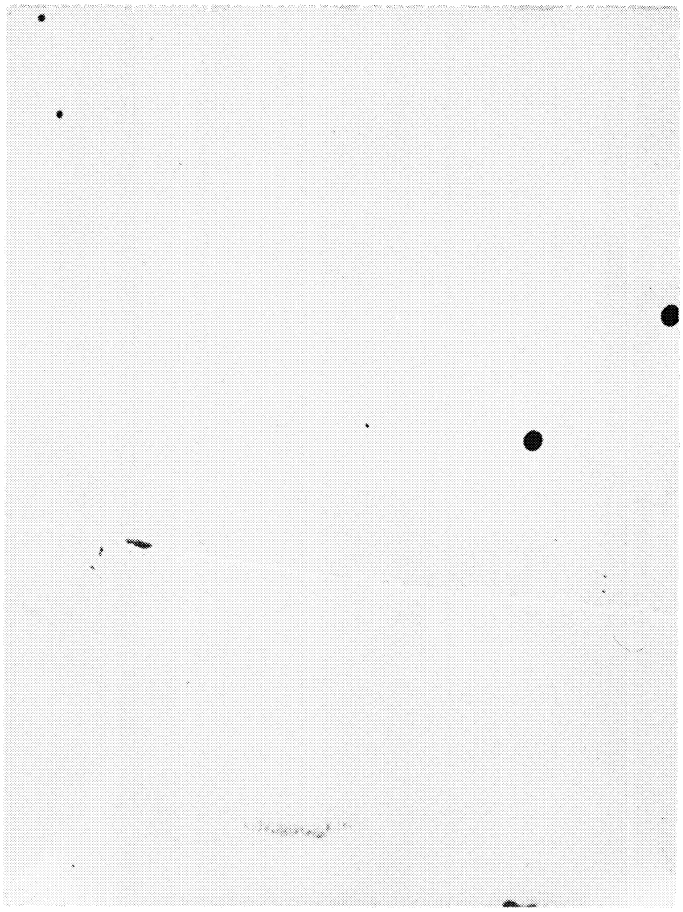

Particle Size: 655Å
Mean Free Path: 1.15 x 10-5
Magnification: 6500X

Figure 25. Fine γ' Dispersion, R 448.

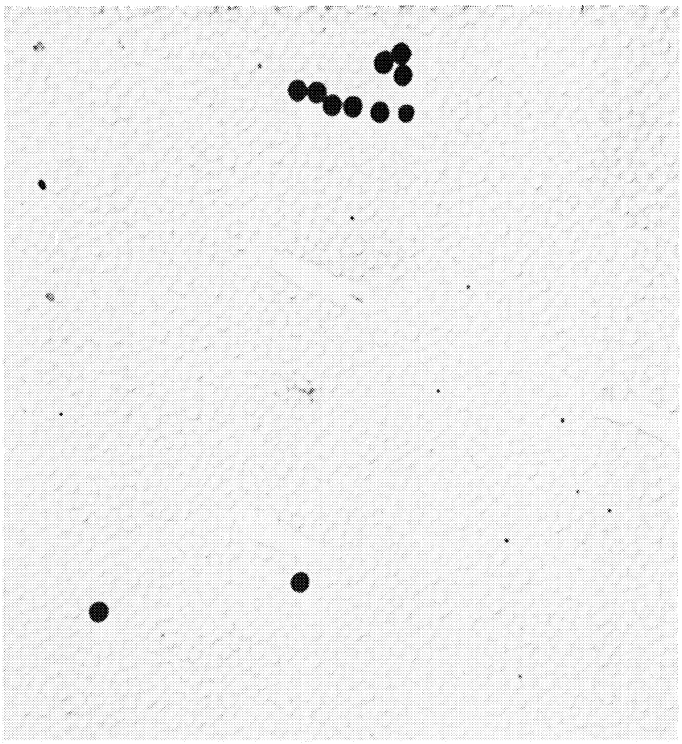

Particle Size: 1200Å
Mean Free Path: 2.15×10^{-5} cm
Magnification: 6500X

Figure 26. Coarse γ' Dispersion, R 448.

BIBLIOGRAPHY

1. Taylor, A., and Floyd, R.W. "The Constitution of Nickel-Rich Alloys of the Nickel-Chromium-Aluminum System." J. Inst. of Metals, 81, (1952-53), 541.

2. Fisher, J.C. "Short Range Order Hardening." Phys. Rev., 91, (1953), 232.

3. Cottrell, A.H. "Interactions of Dislocations and Solute Atoms." Relation of Properties and Microstructure, ASM, (1954), 131.

4. Kornilov, I.I. "Creep of Solid Solutions and Compounds in Metallic Systems." Creep and Fracture of Metals at High Temperatures, London: Her Magesty's Stationary Office, (1956), 215.

5. Herman, M., and Brown, N. "Influence of Order-Disorder Transformation on Creep of Beta Brass." J. of Metals, (May, 1956), 604.

6. Pfeil, L.B., Allen, N.B., and Conway, C.G. "Nickel-Chromium-Titanium-Alloys of the Nimonic 80 Type." High Temperature Steels and Alloys for Gas Turbines, Iron and Steel Institute, London, Special Report No. 43, 1951.

7. Hignet, H.W.G. High Temperature Alloys in British Jet Engines. A lecture presented before the Detroit Chapter of ASM on November 12, 1951, International Nickel Company, Inc., 67 Wall Street, New York, New York.

8. Nordheim, R., and Grant, N.J. "Aging Characteristics of Nickel-Chromium Alloys Hardened with Titanium and Aluminum." J. of Metals, 6, No. 2, (1954), 210.

9. Baille, Y., and Poulignier, J. "Development of a Submicroscopic Precipitate in Hardenable Nickel-Chromium 80-20 Alloys." Comptes Rendus, 237, No. 2, (July 15, 1953), 181-183

10. Baille, Y. "Some Results from Studies with the Electron Microscope of Ni-Cr-Al-Ti Alloys Used in Aeronautical Turbines." Revue Universelle Des Mines, 12, Series 9, No. 10, (Oct. 1956), 507-512.

11. Frey, D.N., Freeman, J.W., and White, A.E. "Fundamental Aging Effects Influencing High-Temperature Properties of Solution-Treated Inconel X." NACA, Tech. Note 2385, June 1951.

12. Mott, N.F., and Nabarro, F.R.N. "An Attempt to Estimate the Degree of Precipitation Hardening with a Simple Model." Proc. Phys. Soc., London, 52, (1940), 86-89.

13. Brockway, L.O., and Bigelow, W.C. "The Investigation of the Minor Phases of Heat-Resistant Alloys by Electron Diffraction and Electron Microscopy." WADC Tech. Report 54-589, May 1955.

14. Betteridge, W., and Smith, R.A. "Effect of Heat Treatment and Structure Upon Creep Properties of Nimonic Alloys Between 750 and 950°C." Symposium on Metallic Materials for Services at Temperatures Above 1600 F, ASTM, (1956), 29.

15. Thomas, J.H., and Davies, R.M. "The Specific Resistance and Temperature Variation of Resistance of Nickel and Some of Its Alloys in the Annealed and Unanealed States." Phil. Mag., 22, (1936 vii), 681.

16. Yano, Z. "Anomaly in the Ni-Rich Solid Solution of the Ni-Cr Binary System." Japan Nickel Review, 9, (1941), 17.

17. Hinkle, J.M. The Thermal Anomaly of the Alloy 80% Ni- 20% Cr (Ni_3Cr). Thesis, University of Michigan, 1948.

18. Grover, H., and Hutqenlaub, G. "The Specific Heat of Ni-Cr Alloys." Phys. Rev., 56, 2, (1939 ii), 212-213.

19. Taylor, A., and Hinton, K.G. "A Study of Order-Disorder and Precipitation Phenomena in Ni-Cr Alloys." J. Inst. Metals, 81, 4, (1952-53), 169-180.

20. Nordheim, R., and Grant, N.J. "Resistivity Anomalies in the Ni-Cr System as Evidence of Ordering Reactions." J. Inst. Metals, 82, 9, (1953-54), 440-444.

21. Roberts, B.W., and Swalin, R.A. "Concerning an Order-Disorder Transition in the Ni-Cr System." Trans. AIME, (July 1957), 845.

22. Weertman, J. "Theory of Creep of Dispersion-Hardened Alloys." Washington, D.C: NRL Report 5123, April 15, 1958.

23. Bragg, W.L., and Williams, E.J. "The Effect of Thermal Agitation on Atomic Arrangement in Alloys." Proc. Roy. Soc., A 145, (1934), 699.

24. Sykes, C., and Evans, H. "The Transformation in the Cu-Au Alloy, Cu_3Au." J. Inst. of Metals, 58, (1936) 255.

25. Borelius, G. "Resistance of Alloys with Disordered and Ordered Arrangements of Atoms." Phys. Soc. of London, 49, (1937), 77-95.

26. Bragg, W.L., Sykes, C., and Bradley, A.J. "A Study of the Order-Disorder Transformation." Proc. Phys. Soc., 49, 274, (1937), 96-102.

27. Jones, F.W., and Sykes, C. "Atomic Rearrangement Process in Cu_3Au, Part II." Proc. Roy. Soc., A 166, 926 (1938), 376-390.

28. Masumoto, M., Sugihara, M., and Tukahashi, M. "On an Anomaly in Specific Heat at Temperature in the Phase Alloys of Ni and Cr." Nippon Kinzoki Gakkai Sci., 78, 2 (1954), 85-87.

29. Kornilov, I.I., and Mints, R.S. "The Compound Ni_3Cr." Doklady Akad. Nauk SSSR, 95, 3, (1954), 543-545.

30. Voss, G. "Alloys of Ni with Sn Pb, Tk, Bi, Cr, Mg_n, Zn, and Cd." Z anorg. Chem., 57, (1908), 58.

31. Bain, E.C. "Crystal Structure of Solid Solutions." Trans. AIME, 68, (1923), 625.

32. Phebus, W.C., and Blake, F.C. "The X-Ray Analysis of Certain Alloys." Phys. Rev., 25, (1925 ii), 107.

33. Blake, F.C., Lord, J.O., and Focke, A.E. "Solid Solutions of Chromium and Nickel, and Iron and Nickel." Phys. Rev., 29, (1927), 206.

34. Smithells, C.J., Williams, S.V., and Avery, J.W. "Laboratory Experiments on High-Temperature Resistance Alloys." J. Inst. Metals, 40, (1928), 269.

35. Nishigori, S., and Hamusumi, M. "Equilibrium Diagram of the Ni-Cr System." Science Reports of the Tohoku Imperial University, 8, (1929), 491.

36. Wever, F., and Jellinghaus, W. "Das Dreistoffsystem Eisen-Chrom-Nickel." Mitteilungen aus dem Kaiser-Wilhelm Institut fur Eisenforschung, 13, (1931), 93.

37. Matsunaga, B. "Ni-Cr Alloy." Japan Nickel Review, 1, (1933), 347.

38. Jenkins, C.H.M., Bucknall, E.H., Austin, C.R., and Mellor, C.A. "Some Alloys for Use at High Temperatures, Part IV - The Constitution of the Alloys of Nickel, Chromium, and Iron." J. Iron Steel Inst., 136, (1937), 193.

39. Bloom, D.S., and Grant, N.J. "Chromium-Nickel Phase Diagram." Trans. AIME, 191, (1951), 1009.

40. Gwyer, A.G.C. "Alloys of Al with Cu, Fe, Ni, Co, Pb, and Cd." Z anorg. Chem., 57, (1908), 133.

41. Bradley, A.J. "An X-Ray Analysis of the Ni-Al System." Proc. Roy. Soc., A 159, 896, (1937), 56-72.

42. Alexander, W.O., and Vaughn, N.B. "The Constitution of the Ni-Al System." J. Inst. Metals, 61, (1937), 247-260.

43. Schramm, J. "The Binary System Ni-NiAl." Z. Metallkunde, 33, 10, (1941), 347-355.

44. Groeber, H., and Hauk, V. "The Al-Ni Equilibrium Diagram." Z. Metallkunde, 41, 8, (1950), 283-284.

45. Kornilov, I.I., and Mints, R.S. "Melting Diagram of the System Ni-Cr-NiAl." Doklady Akad. Nauk SSSR, 94, 6, (1954), 1085-1088.

46. Floyd, R.W. "The Formation of Ni_3Al Phase in Ni-Al Alloys." J. Inst. Metals, 80, 10, (1951-52), 551-553.

47. Taylor, A., and Floyd, R.W. "The Constitution of Nickel-Rich Alloys of the Ni-Ti-Al System." J. Inst. Metals, 81, 1, (1952-53), 25-32.

48. Byrne, P.J.S., and Hansen, H.L. "Preparation of Powder Samples for Use in Focusing Cameras." Norelco Reporter, 3, (1956), 107.

49. Klug, H.P., and Alexander, L.E. X-Ray Diffraction Procedures. New York: John Wiley and Son Inc., 1954.

50. Bigelow, W.C., Amy, J.A., and Brockway, L.O. "Electron Microscopic Identification of the γ' Phase of Nickel-Base Alloys." Proc. ASTM, 56, (1956), 945.

51. Howard, R.T., and Cohen, M. "Quantitative Metallography by Point-Counting and Lineal Analysis." Trans. AIME, Iron and Steel Division, 172, (1947), 413.

52. Flinn, P.A. "An Investigation of the Properties of Ni-Al-Fe Alloys Based on Ni_3Al." Research Report 60-94701-2-R1, Pittsburgh, Pa: Westinghouse Research Laboratories.

53. Orowan, E. "Dislocations and Mechanical Properties." Dislocations in Metals, AIME, (1954) 69.